A Comparison of Experiment and Analysis for a Ducted Propeller

by

Michael J. Hughes

B.S., Webb Institute of Naval Architecture (1988)

Submitted in Partial Fulfillment of the Requirements

for the Degree of Master of Science in Ocean Engineering

at the

Massachusetts Institute of Technology

May, 1990

Signature of Author _____
Department of Ocean Engineering
May, 1990

Certified by _____
Professor J.E. Kerwin
Thesis Supervisor

Accepted by _____
Professor A. Douglas Carmichael
Chairman, Department Graduate Committee

A Comparison of Experiment and Analysis for a Ducted Propeller

by
Michael J. Hughes

Submitted to the Department of Ocean Engineering on May 11, 1990
in partial fulfillment of the requirements for the Degree of
Master of Science in Ocean Engineering

Abstract

A duct was designed to operate efficiently with a given stock propeller. The objective for the ducted propeller was to maintain the propeller at its ideal angle of attack while ensuring that the duct provided some thrust without flow separation occurring on the duct. The design procedure involved the use of the Ducted Propeller Steady Flow 2 (DPSF-2) computer code. This code utilizes a potential based surface panel method to analyze the duct and hub and a vortex lattice method to analyze the propeller.

The duct was then built and tested in the MIT water tunnel. Experimental results were obtained for the forces on the duct and propeller over a range of advance coefficients. The velocities were measured in the field in front of and behind the duct using a laser doppler velocimetry system. Using these velocities the experimental values for the spanwise distribution of circulation on the propeller blades was then calculated.

The results were then compared to the results from the analysis code over the same range of advance coefficients showing good agreement for the duct and propeller forces and the circulation in the region of attached flow. The effect of the duct on the performance of the propeller is also shown from the experimental data.

Thesis Supervisor: Professor Justin E. Kerwin

Title: Professor of Naval Architecture

Aknowledgements

I would like to acknowledge Dr. Spyros Kinnas and Professor J.E. Kerwin for their encouragement, enthusiasm and guidance during all phases of this research. I would also like to thank the rest of the propeller group for their continuous support, technical and otherwise.

I also wish to thank Mr. Peter Sebelius and Mr. John Chiffer of Draper Laboratory for their valuable comments and discussion during the course of this work. This research was sponsored in part by the Charles Stark Draper Laboratory Internal Research and Development Program. I also express my thanks to the Society of Naval Architects and Marine Engineers, whose scholarship helped support the first year of my studies at MIT.

Finally, I would like to thank Mom and Dad for everything they've done for me.

Contents

List of Figures

List of Tables

Chapter 1

Introduction

The objectives of the research performed for this thesis were to perform an extensive experiment on a ducted propeller in different flow conditions and measure the forces and flow-field velocities around it. These measurements were then used to validate the performance of an existing Ducted Propeller Steady Flow (DPSF2) analysis method for ducted propellers operating both at and away from the design operating condition.

There are two basic types of ducted propellers. The first of these is the accelerating nozzle. This type of duct came into use during the 1930's. Work performed by Kort in 1934 showed that an increase in efficiency can be gained through the use of a duct for heavily loaded propellers. This type of duct is often referred to as a "Kort nozzle." It has also been observed that the optimum diameter for a ducted propeller is less than that for an open propeller providing the same thrust. The ducted propeller with an accelerating duct has been used extensively in cases where the propeller is highly loaded or of limited diameter. In this configuration. the circulation around the duct is such that the duct itself produces thrust. This type of ducted propeller also performs extremely well in the bollard pull condition. This makes the ducted propeller well suited for vessels such as tugboats and trawlers which often operate at near zero speed with heavily loaded propellers. The ducted propeller has the additional advantage in

that it protects the propeller from debris and from striking fixed objects such as the bottom or banks. This can be helpful for vessels operating in shallow or restricted waters. These factors also make ducted propellers attractive for remotely operated and autonomous underwater vehicles. Ducted propellers of the accelerating type have also been used on large tankers and cargo ships for which a large thrust is required at a given propeller diameter. There has also been some attention focused on the use of ducted propellers for higher speed naval applications.

The second type of ducted propeller configuration is the decelerating nozzle. In this configuration the duct is used to increase the static pressure at the propeller. This type of ducted propeller is used in order to retard propeller cavitation and can result in a reduction in the noise generated at the propeller. The decelerating ducted propeller is also known as the "pumpjet." In this case, however, the circulation around the duct is such that the duct produces a negative thrust, decreasing the efficiency of the system.

Various methods exist for the design and analysis of ducted propellers. One of the principle methods concerns the use of data from systematic experiments performed at the Netherlands Ship Model Basin (N.S.M.B.). There are also theoretical methods available for ducted propellers. In all of the theoretical models known to this author the assumption is made that the duct and propeller may be treated as independent devices. The effects of the duct on the propeller and of the propeller on the duct are then computed in an iterative manner. The assumption of an inviscid and incompressible fluid is also made. Many of these theoretical models are based on linearized theory and on axisymmetric nozzles in uniform flow. In linearized theory the duct is represented by a distribution of ring vorticies and ring sources along a constant diameter cylinder, and a linearized boundary condition is imposed. The propeller in these models is either treated as an actuator disk or with a lifting line model. These methods, however, can not accurately predict whether flow separation occurs on the duct, as may happen if

the duct is heavily loaded or not at its ideal angle of attack.

Several attempts have been made to model ducted propellers using non-linear theory. An example of one of these methods is the DPSF program developed at MIT. This program was a predecesor to the DPSF-2 program used in this work. In the original version of DPSF the duct and propeller were both modeled by single straight-line vortex and source elements of constant strength, distributed over the mean camber surface. A more complete description of this program is provided in reference [11]. An earlier method incorporating non-linear theory was developed by Ryan and Glover [3]. This method models the duct with a continuous distribution of vortex rings on the duct profile. The propeller is modelled with a finite number of lifting lines with associated helical vortex sheets. Another method incorporating non-linear theory was put forth by Gibson and Lewis [1]. Their model utilizes surface vorticity analysis for the duct with an actuator disk representation of the propeller.

In [5] a potential based panel method has been utilized for the representation of the duct and, a vortex lattice lifting surface method for the representation of the propeller. The corresponding computer code, DPSF-2, is described in [6]. Detailed non-axisymmetric pressure distributions on the duct as well as the duct thrust have been produced as a result of this method. The method was subsequently extended to determine the optimum loading of a propeller inside a given duct with the duct represented in non-linear theory [7]. This was further developed to form a design method for a ducted propeller using a systematic technique for designing the propeller as well as the duct [8]. The numerical validation of DPSF-2, i.e. comparison with analytic results for simple configurations and convergence with number of panels, has been established and is documented in [5].

The work done in this thesis attempts to to complete the validation of DPSF-2 by comparison with experimental results. In lack of detailed flow field measurements

around a ducted propeller model, an experiment was performed at the MIT water tunnel. A duct was designed for an existing propeller along with an apparatus to test this ducted propeller system in the MIT variable pressure water tunnel. Both force measurements and LDV velocity measurements were carried out on this model. The panel method, DPSF-2, was then used to analyze some of the operating conditions studied in the tests. This thesis includes a description of the duct design, a description of the experimental procedure and the theoretical calculations. and a discussion of both the theoretical and experimental results with a comparison between the two. Comparisons are also made between the experimental results from the ducted propeller and the same propeller operating without a duct.

Chapter 2

Duct Design Procedure

In order to perform the experimental investigation a ducted propeller model was needed. It was most efficient to design a duct which would be well suited to an existing propeller which could be obtained free of cost. A propeller was chosen from the archives at the MIT propeller tunnel. In this manner a ducted propeller model could be obtained at an affordable cost. A complete description of the geometry of the duct and propeller is given in appendix A.

As a first step the design condition for the propeller operating alone was determined. This was done using the PSF-2 program (Propeller Steady Flow - 2). This program uses a vortex lattice method to solve the propeller boundary value problem. The chosen propeller had a parabolic camber distribution for which the ideal chordwise distribution of loading is well known. The advance coefficient for the given propeller geometry was varied within the PSF-2 program until the chordwise distribution of vorticity over the propeller blade sections matched that of an airfoil with a parabolic mean line operating with shock free entry. This occurred at an advance coefficient of about 0.4. Then an experiment was performed, and a comparison of the forces obtained from PSF-2 and the experimental forces for the open propeller is shown in figure 2.1.

Now that the propeller's operating conditions had been determined it was neccesary

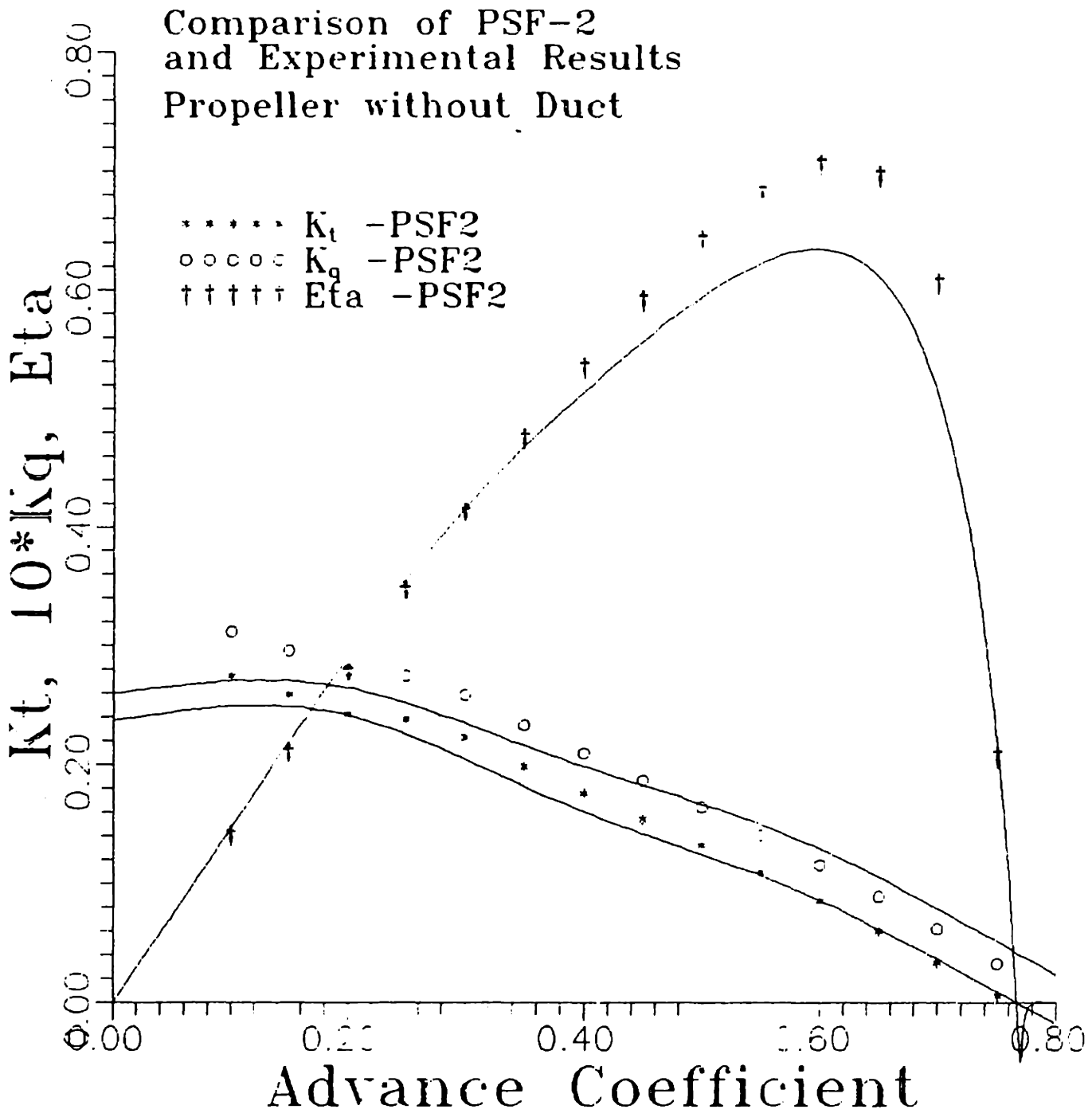

Figure 2.1: Comparison of analysis and experiment for open propeller

to design a duct which would opperate effectively in combination with the propeller. The objectives of the duct design process were: (1) to maintain the propeller blade sections at their ideal angle of attack in the presence of the duct, and (2) to produce some positive thrust to overcome the duct viscous forces while ensuring that the flow around the duct remained unseparated over a large range of operating conditions.

Several characteristics of the duct had to be fixed at the start of the design in order to limit the number of possible variations in the duct geometry. These parameters were established according to what we felt were typical values for a ducted propeller which would be used for a UUV. The size of the gap between the tip of the propeller and the duct was chosen to be 2.5% of the propeller radius. The duct chord length was chosen to be equal to the propeller radius and the thickness of the duct cross section was set at 12% of the duct chord. The axial position of the propeller within the duct was fixed at 60% of the duct chord aft of the duct leading edge. The propeller was placed slightly aft of center in order to allow room for the struts neccesary to support the duct. The algorithm chosen to determine the shape of the duct was a B-spline routine which has been used previously to design propeller blade sections. This in effect set the camber and thickness form of the duct cross section. The entire duct geometry, therefore, is established by giving the maximum camber and thickness over the duct cross-section and the angle of attack of the cross-section. Since a slightly accelerating duct was desired, an advance coefficient of 0.3 was chosen for the ducted propeller. Of course the strictest contraint on the design of the duct was that the propeller geometry was completely fixed. There were two remaining parameters which could then be varied in order to achieve the design objectives. These variable parameters were the camber and angle of attack of the duct cross section. These two parameters are described in fig. 2.2.

A duct with a geometry similar to existing ducts was then added to use as a starting

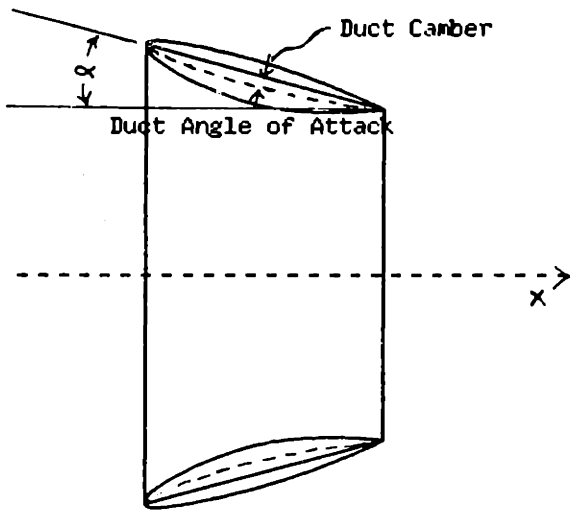

Figure 2.2: Definition of duct camber and angle of attack.

point for the duct design. The geometry of this first iteration cross section is shown in figure 2.3a. The analysis of the flow around this configuration was then obtained using the DPSF-2 program (Ducted Propeller Steady Flow 2). This program will be described in more detail in a later section. It was discovered that the presence of the duct significantly accelerated the flow at the propeller, resulting in the propeller blades no longer operating at an ideal angle of attack. This could be seen from examining the chordwise distribution of bound vorticity shown in figure 2.4a. It can be seen that there is a large amount of negative loading near the leading edge of the propeller blades. This indicates that the advance coefficient based on the local velocity at the propeller plane was significantly above the design advance coefficient of the propeller resulting in a need to decrease the extent to which the duct accelerates the flow past the propeller. However, this was not the only problem with this first iteration duct; in addition, the pressure distribution for this first duct iteration showed a large negative pressure peak near the leading edge of the duct on the interior surface (see fig. 2.5a).

a.) First iteration duct profile

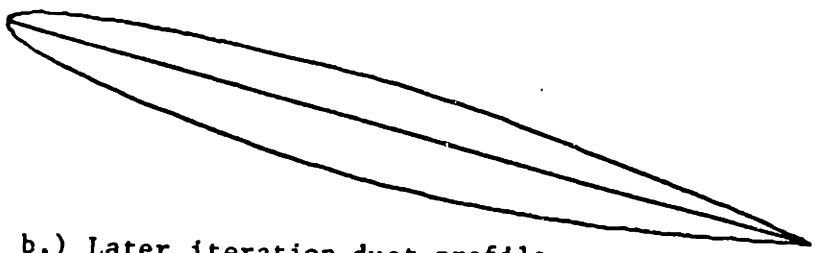

b.) Later iteration duct profile

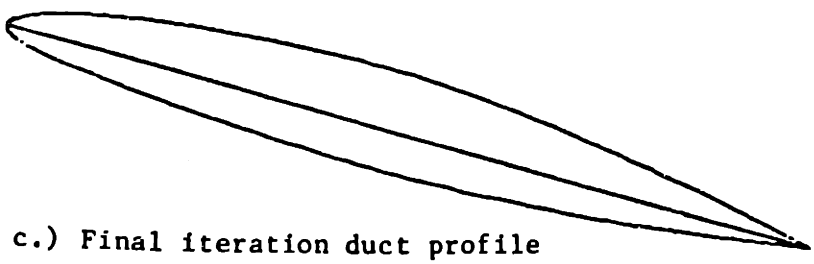

c.) Final iteration duct profile

Figure 2.3: Duct cross-section profiles

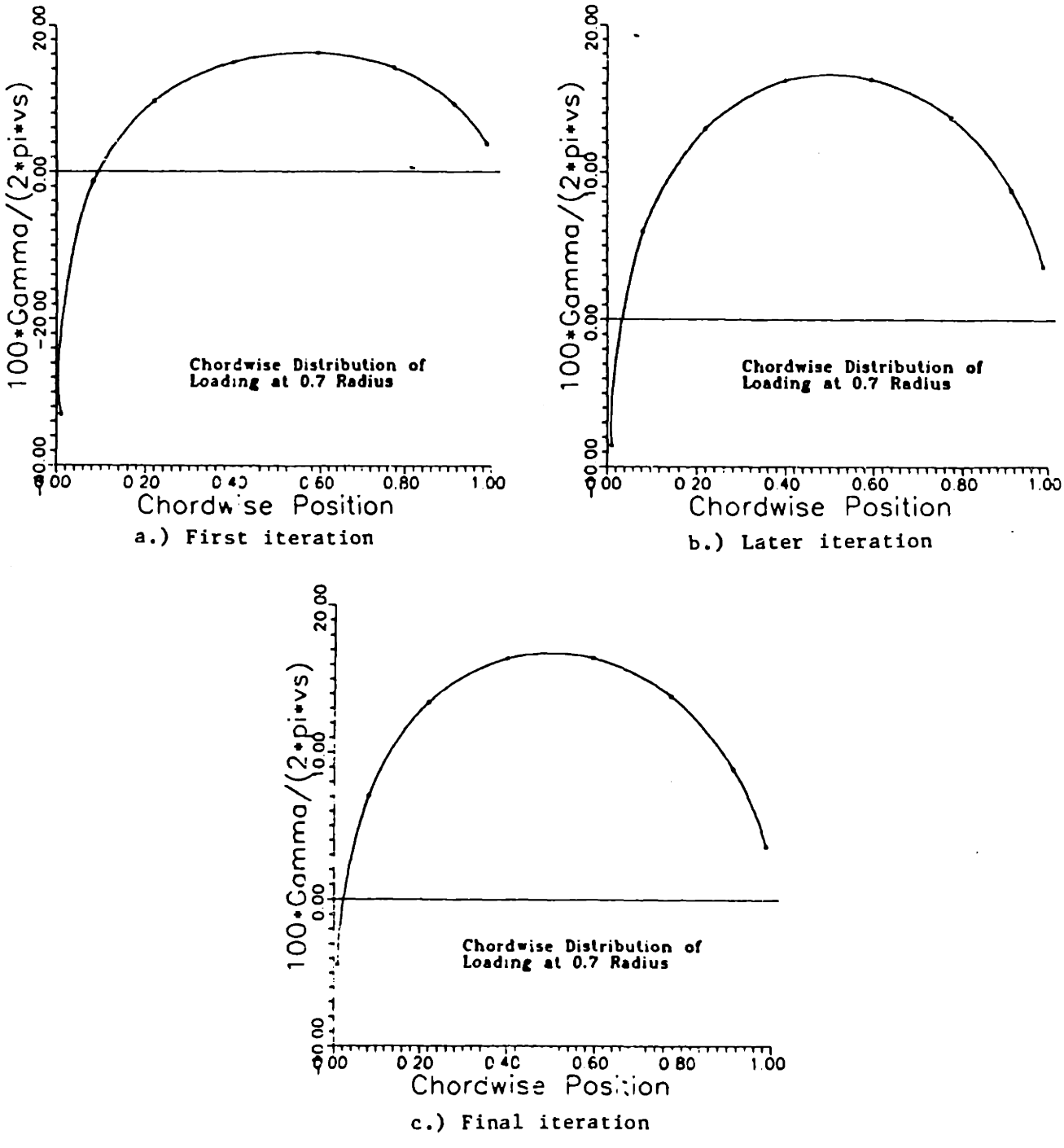

Figure 2.4: Chordwise distribution of loading at 0.7 radius on propeller blade.

This indicated that the duct was operating far below its ideal angle of attack and that separation would occur on the inside surface near the leading edge.

The next several duct iterations attempted to find the correct angle of attack for the duct. For these iterations a duct with only a small amount of camber was used and only the angle of attack was varied. From these iterations it was determined that the duct cross section would have a satisfactory pressure distribution (i.e.. operate near ideal angle of attack) at angles of attack between 13 and 16 degrees. The geometry of the duct cross section which existed at this stage of the design is shown in fig. 2.3b. It was later speculated that a reasonable first attempt for this angle could have been obtained more easily by calculating the angle of the streamlines present in the flow of the propeller without the duct, and then placing the duct along these streamlines.

Although the negative pressure peak at the leading edge of the duct was now eliminated, the propeller was still away from its optimum operating point (see fig. 2.4b and fig. 2.5b). This indicated that the flow through the duct was still being accelerated too much, and the propeller was operating at a higher advance coefficient than that for which it was designed. In order to correct this situation the camber on the duct cross section was reduced in order to reduce the circulation around the duct. Several more iterations were required to obtain the best combination of camber and angle of attack for the duct cross section. The geometry of this final duct iteration is shown in fig. 2.3c. In the end, negative camber was required in order to produce a flow field satisfactory to the propeller. Although negative camber would tend to produce circulation in a direction which would decelerate the flow, the flow into the propeller was still accelerated because of the angle of attack of the duct. The selection of negative camber was necessary because the propeller had a low pitch (P/D approx. 0.6). If both the propeller and the duct were being designed, the pitch of the propeller blades could be increased to match the flow produced by the duct, but in this case the duct

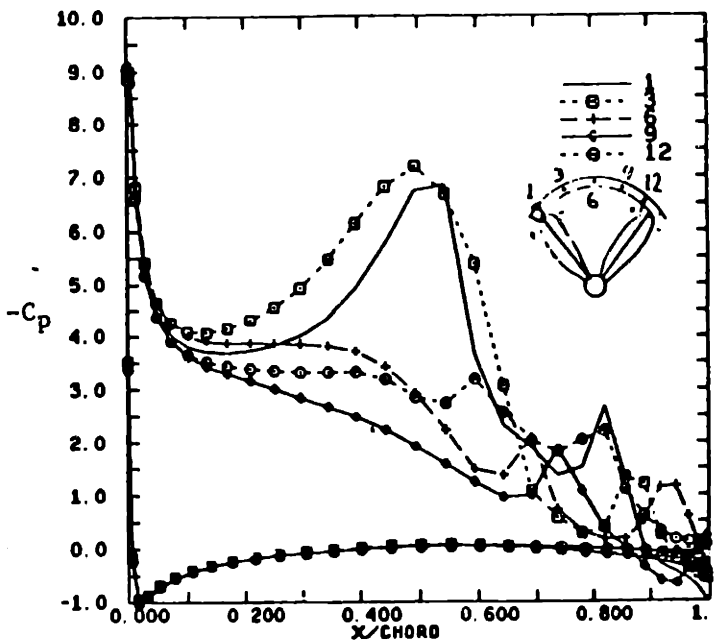

a.) First iteration - Pressure distribution on duct.

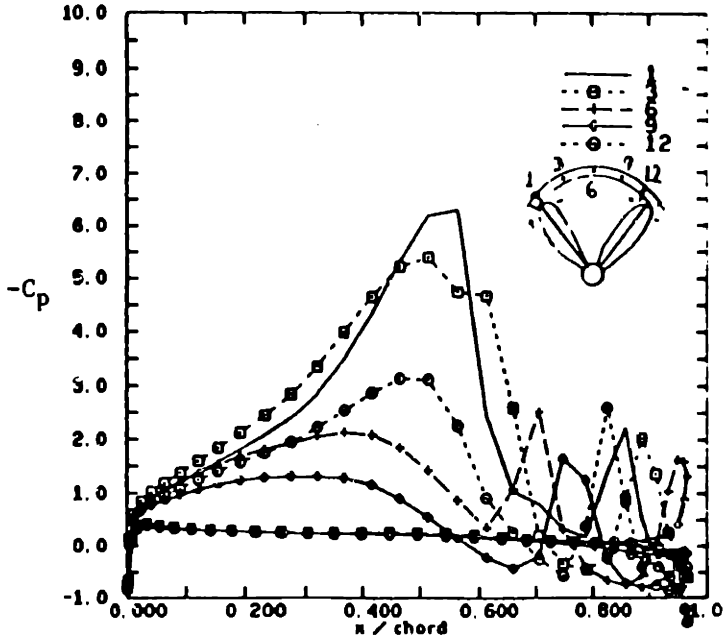

b.) Later iteration - Pressure distribution on duct.

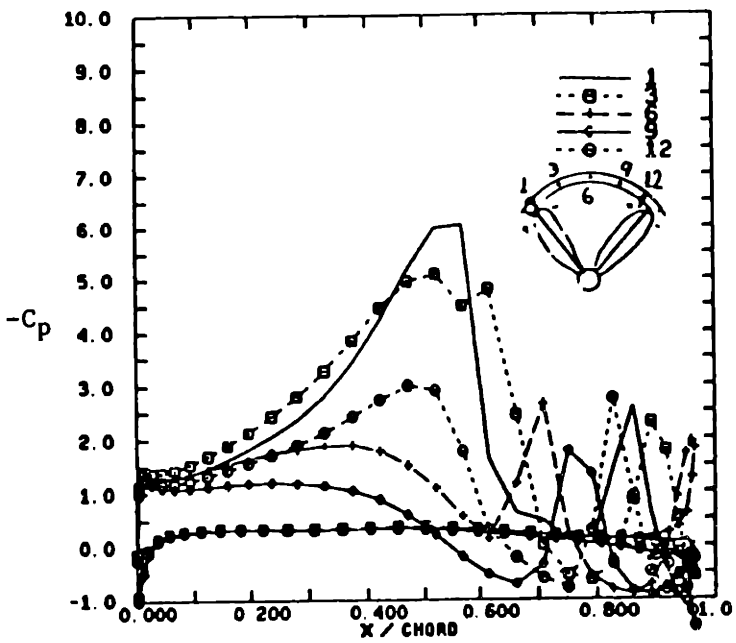

c.) Final iteration - Pressure distribution on duct.

Figure 2.5: Chordwise distribution of pressure on the duct cross-section at different circumferential positions within two consectutive blades.

had to be adjusted to produce a flow satisfactory for a given propeller geometry. The pressure distribution and cross section for the final duct iteration is shown in figures 2.4c and 2.5c respectively.

We have recently completed the design of a duct for a more highly pitched propeller, which will be tested by the time this paper is completed. This duct was designed using the same procedure describe above, except that the effects of a set of pre-swirl stator vanes were included in the design. For this propeller duct combination, however, the duct angle of attack is only six degrees and the camber is in the expected direction.

Chapter 3

Experimental Procedure

An apparatus was developed to hold the duct to the propeller shaft in the MIT variable pressure water tunnel. This apparatus was designed to allow for two configurations. In one configuration the forces on both the duct and propeller are measured by the propeller dynamometer and in the second configuration only the propeller forces are measured. The apparatus consists of a sleeve which slides over the outer non-rotating shaft in the propeller tunnel. A drawing of this apparatus is shown in fig. 3.1. The upper half of the drawing shows the first configuration in which the sleeve floats on the outer propeller shaft and is connected to the propeller dynamometer through a thrust bearing. The lower half of the drawing shows the second configuration in which the thrust bearing has been removed and the sleeve is clamped to the outer propeller shaft using a series of set screws. The duct is connected to this sleeve by four symmetric struts located upstream of the propeller.

Using this apparatus experiments were performed throughout the month of June 1989. The duct was manufactured from a transparent plastic in order that the propeller could be observed during the experiment. By saturating the water in the tunnel with air bubbles, the streamlines along the duct on both the inside and the outside could be observed. This showed that the flow around the duct remained unseparated over a wide

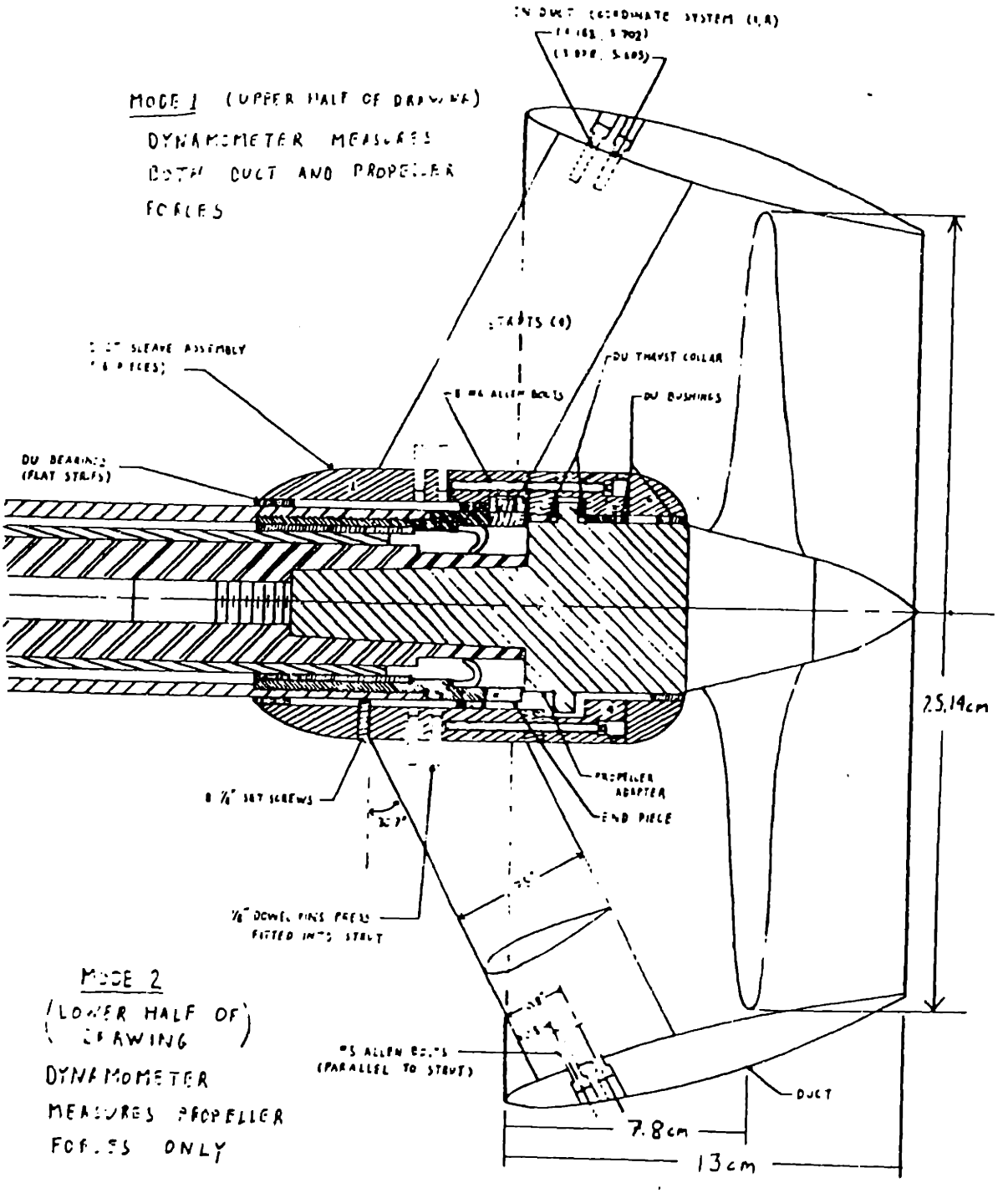

Figure 3.1: The experimental apparatus

range of conditions ranging from advance coefficients of 0.1 to 0.5. This indicates that the duct truly is operating near its ideal angle of attack at the design advance coefficient of 0.3. Force measurements were made over a wide range of advance coefficients in both the ahead and astern conditions. These measurements were made first using the configuration in which only the propeller forces are measured and then using the configuration in which the combined forces on the duct and propeller are measured. In this manner the forces on the duct alone could be obtained by simply subtracting the forces measured in each of the configurations. Force measurements were also made for the propeller without the presence of the duct. For this test the duct sleeve without the struts was left in the tunnel to insure that both the ducted propeller and non-ducted propeller would have the same hub arrangement. A complete listing of the results for all the open water tests performed is given in appendix E.

Measurements of the velocity field behind and in front of the duct were taken using the Laser Doppler Velocimetry system. The velocity measured was the circumferential mean velocity obtained by recording the time average of the velocities measured at a specified axial location and radius. Measurements at different radii of the axial, radial, and tangential velocity were taken at three axial positions aft of the duct trailing edge. This was done for five advance coefficients. The axial velocity as a function of radial position was also measured at two axial positions upstream of the duct for two advance coefficients. The locations at which the velocity measurements were made are shown in fig. 3.2. For this part of the experiment an empty wake screen holder, consisting of four cross struts, was placed about three feet upsteam of the duct in order to prevent any vibrations which could effect the velocity measurements.

Flow measurements were also performed behind the duct without the propeller present. This was done in order to verify the first iteration of the DPSF-2 code in which the problem of the duct alone is solved. However, without the propeller present

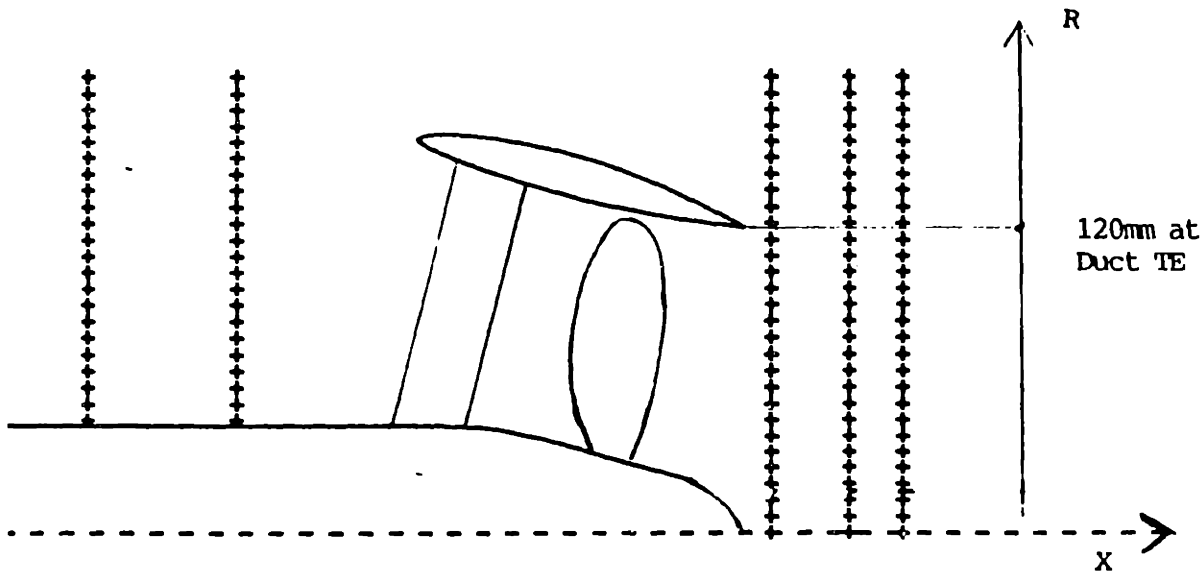

Figure 3.2: Location of LDV velocity measurements

the duct flow was found to be separated even at very low speeds. This separation was discovered through the measurement of near zero velocities near the outer surface of the duct near the trailing edge. The duct does not separate, however, when the propeller is present, because the duct was designed to operate in the propeller flow field.

From the values of the tangential velocity in the wake of the duct it was possible to determine an experimental value for the spanwise distribution of circulation on the propeller blades. This was done by applying Kelvin's theorem to the propeller problem. The method used to measure the velocities and determine the circulation is described in detail by Wang in [9] and will not be restated here.

In order to calculate the proper value of the inflow velocity with which to non-dimensionalize the measured velocities, the effects of the tunnel wall had to be taken into account correctly. When measuring the forces, the tunnel wall was accounted for using the principles of momentum and continuity in a linearized manner to determine

the corrected value for the advance coefficient and K_t, as described in [2]. The velocities measured using the LDV system were non-dimensionalized with respect to the velocity corresponding to the corrected value of the advance coefficient at the same rpm. This results in a discrepancy in the axial velocities outside the propeller/duct slipstream aft of the duct. The values of the velocities in this region calculated by the analysis code approach free stream as the field point moves away from the propeller/duct slipstream. This is of course what is expected because there is no tunnel wall modelled in the analysis. However, in the case of the experiment, the presence of the tunnel wall modifies these velocities. The principle of momentum forces the flow in the propeller/duct slipstream to be accelerated when thrust is being produced. The principle of continuity, however, forces the flow outside the slipstream to be decceleratated so that the mass flow through the tunnel is conserved. This, however, does not apply to the analysis code where no tunnel wall is present. The authors are currently working on a better method of including the effects of the tunnel wall in the analysis of ducted propellers.

Chapter 4

Theoretical Calculations

Theoretical computations were performed using the DPSF-2 program. In DPSF-2 the flow around the duct and the hub is solved via a discretized boundary integral method, or *panel method*. The duct and the hub are treated as a single unit. The propeller is modelled by a lifting surface method. The duct and the propeller are treated as independent devices. However, the effects of the duct on the propeller and of the propeller on the duct are computed in an iterative manner. The assumption of an inviscid and incompressible flow is also made. A complete description of the DPSF-2 program is provided in references [5] and [6]. In the original version of this code the grid of the panels on the duct was set up to match the pitch of the propeller blades at propeller tip in order to reduce numerical errors. However, in this case the propeller had a very low pitch and a rounded tip which resulted in very elongated, oddly shaped panels being formed on the duct. At the same time, the relatively large gap between the tip of the propeller and the duct made the alignment of these two grids less important. For this reason the program was modified to have the option of paneling the duct with a different pitch from the propeller tip. Sixty circumferential and sixty-two spanwise panels were used when modeling the duct. For the propeller eight chordwise and eight spanwise vortex segments were used. The resulting panel arrangement can be seen in

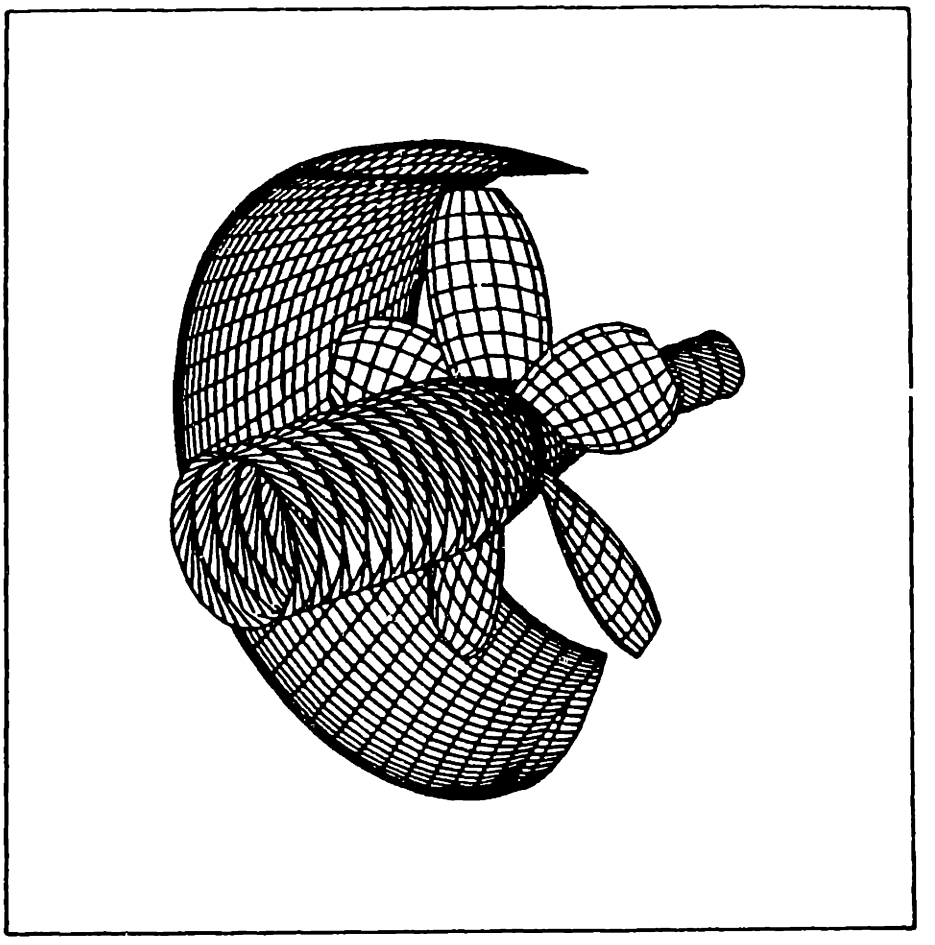

Figure 4.1: Panel arrangement for propeller, duct, and hub

figure 4.1. A larger number of panels was used on the hub than is shown in the figure. The sleeve apparatus which holds the duct was modelled as part of the hub. This configuration was used to calculate the forces on the ducted propeller over a range of advance coefficients. For most of the DPSF-2 runs nine iterations were used for the duct and propeller solutions. However, at very low advance coefficients, eleven iterations were required in order to achieve adequate convergence.

The output from the theoretical calculations consists of K_t and K_q for the propeller, the velocities at the plane of the propeller, the pressure distribution over the duct, and the circulation on the duct and propeller. The circulation distributions calculated in the chordwise and spanwise directions are given in appendix C. Examples of the pressure distributions at two advance coefficients are shown in figure 4.2. The pressure

distributions for all of the advance coefficients for which calculations were performed are included in appendix D. DPSF-2 also calculates a non-dimensionalized force coefficient for the duct by integrating the pressure distribution. This is converted to a K_t value for the duct in order to compare against experimental results. The viscous drag on the duct is taken into account by assuming that the drag coefficient of the duct profile is 0.0085. Although the propeller was modelled with a vortex lattice, the forces on the propeller were calculated using lifting line theory, where the circulation at the control point radii on the lifting line was taken to be the sum of the vorticity at the chordwise control points at that radii.

The program was extended to calculate the velocity at any point in the flow field after the solution has been achieved. As with the experimental case, the velocity calculated is the mean circumferential velocity at a given axial location and radius. This value is obtained, however, by first calculating the velocities at a series of angular positions and taking the average of these values. It is essential to avoid computing the velocity at points in the vicinity of the propeller and duct panels, where the discretization error is substantial. The velocities are obtained by calculating the induced velocity from the duct and propeller separately and adding these two velocities to the inflow velocity. The propeller induced velocities were calculated based on the strength of the propeller vortex lattice elements. The method used to calculate these velocities is documented in reference [4]. The duct induced velocities were calculated by superimposing the velocities due to the dipole and source panels on the duct and its wake. This procedure is described in more detail in Appendix B.

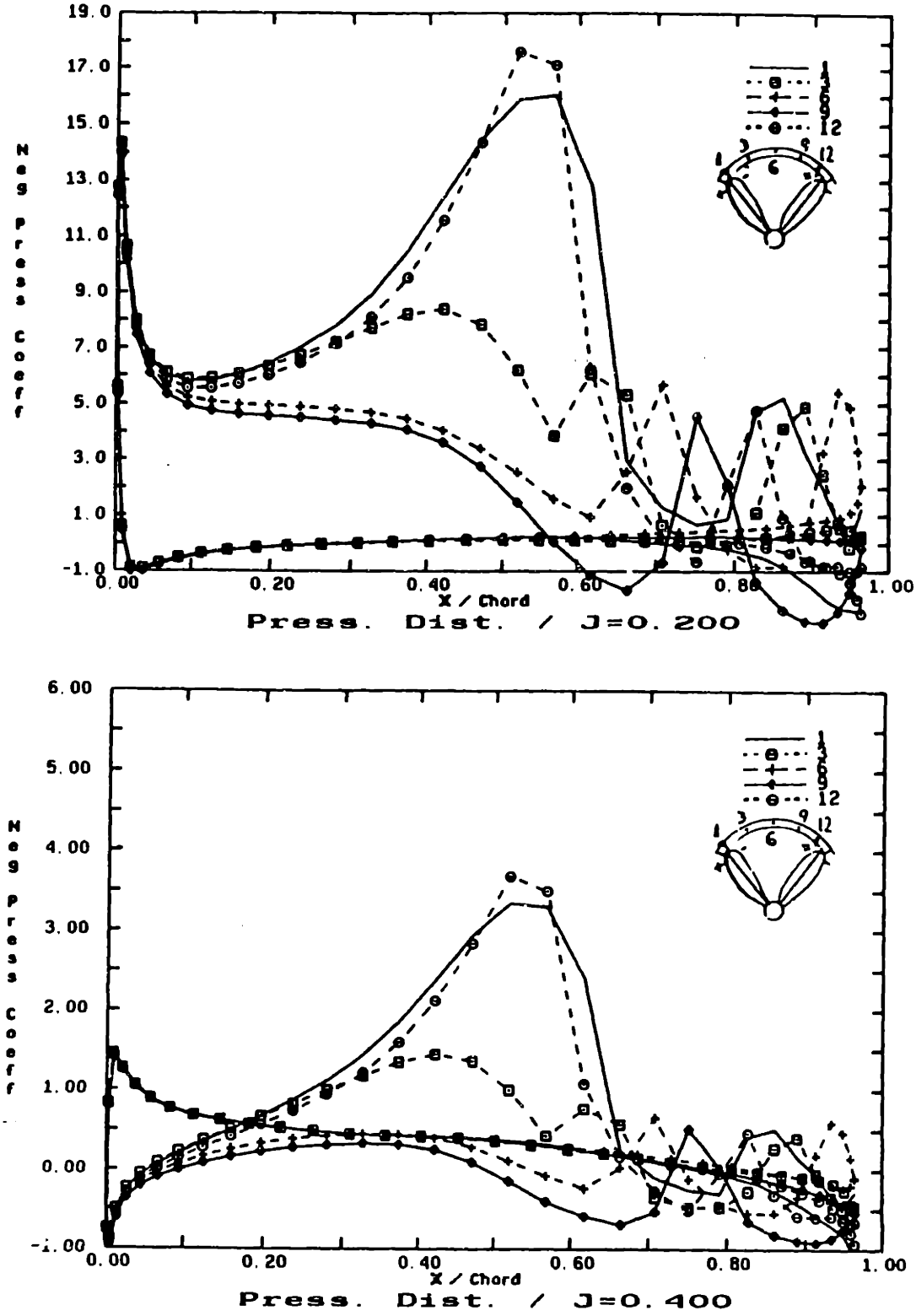

Figure 4.2: Duct pressure distributions at off-design conditions, shown at different circumferential positions within two consectutive blades.

Chapter 5

Comparison of Theoretical and Experimental Results

Open water curves in both ahead and astern conditions were obtained experimentally for the case of the forces on the propeller without the duct, the forces on the propeller in the presence of the duct, and the combined forces on the duct and propeller. A comparison between the experimental results for the open propeller and the ducted propeller is shown in fig. 5.1. It can be seen that the ducted propeller has a higher efficiency at advance coefficients from 0 to 0.41. At the design advance coefficent of the ducted propeller, 0.3, the gain in efficiency is about ten percent. Both the values for K_t and K_q are lower for the ducted propeller over the complete range of advance coefficients. This is caused by the duct accelerating the flow into the propeller making the advance coefficient based on the local flow at the propelller higher than that based on the incoming flow. The result is that the K_t and K_q curves are shifted to the left when the duct is present. It must be pointed out that this comparison is not a good indicator for the merits of using a ducted propeller, as the propeller chosen was not designed to operate with a duct. It can be seen that the curves for K_t and K_q are much flater than would be typical for an open propeller. This indicates that the performance of the ducted propeller depends very little on advance coefficient over this

region. The comparison between the astern condition for the ducted propeller and the same propeller without a duct is shown in figure 5.2. In this condition the efficiencies of the ducted propeller and the open propeller are almost identical. In this case, however, the magnitudes of K_t and K_q are higher for the ducted propeller, because the duct still tends to shift the K_t and K_q curves to the left. No comparison to a theoretical value for the astern performace of a ducted propeller is given. When operating in the astern condition the majority of both the propeller and the duct are working in separated flow. At the present time, an adequate method for calculating the flow and forces produced by a propeller in separated flow is not currently available in the DPSF-2 program.

A comparison between the experimental results and the results from DPSF-2 is shown in figures 5.3 and 5.4. Figure 5.3 shows the results for the forces measured on the propeller alone in the presence of the duct compared with the same forces from DPSF-2. Figure 5.4 shows the same comparison including the forces on the duct. It can be seen in fig. 5.3 that the K_t and K_q for the propeller are predicted very accurately over the full range of advance coefficients. The value for K_t on the duct is slightly over-predicted at all values of advance coefficients; although the shape of this curve is predicted correctly. This could possibly be due to separation occuring on the inside of the duct aft of the propeller. The pressure distribution on the duct shows a negative pressure gradient aft of the propeller which indicates that the flow might separate here. This would tend to decrease the thrust produced by the duct. The overprediction of duct thrust results in the total thrust and open water efficiency predicted by DPSF-2 being slightly higher than the experimental result. Overall, however, the results show a very good correlation between the theory and experiment.

The values from the LDV flow mappings are plotted in figures 5.5 - 5.9. The measurements of the axial velocities upstream from the propeller showed the flow to be uniform, except for the presence of the shaft boundary layer, and equal to the tunnel

velocity measured using the differential pressure cell. The upstream axial velocities are shown in fig. 5.5. The axial velocities behind the duct indicated that the flow was accelerated through the duct as expected. As the point where the velocity was being measured moved downstream from the trailing edge of the duct, the axial component of the velocity increased while the radial component of the velocity decreased and the tangential component remained roughly the same. This is what is expected as the angle of the streamlines in the flow aft of the duct decrease as the flow moves downstream. The velocities measured aft of the duct at two different values of advance coefficient are shown in figures 5.6 and 5.7. The trailing edge of the duct has a radius of 12 cm. Figure 5.8 show a comparison between the axial and tangential velocities measured one centimeter behind the trailing edge of the duct and those calculated using DPSF-2 at J=0.3. Figure 5.9 shows the same comparison for J=0.373. In both cases the correlation is relatively good although there is a discrepancy in the comparison of the axial velocities. This can be attributed to the effect of the tunnel wall on the velocities in this region as was discussed in section 3. The shape of the curve for the axial velocities is accurately predicted, but the values obtained from DPSF-2 are shifted higher by a consistant amount over the span. It is interesting to note that the magnitude of this shift is roughly equivalent to the discrepancy between the velocity measured outside of the propeller/duct slipstream and the free stream velocity. This indicates that the discrepancy might disappear if a more systematic method of accounting for the tunnel wall effects were incorperated into the program. The tangential velocities do not experience this problem because the tunnel wall has little effect on the tangential component of the velocity.

From the values of tangential velocity versus radial position, the radial distribution of circulation around the propeller can be calculated. A comparison was also made between the spanwise distribution of circulation calculated from DPSF-2 and that

obtained from the tangential velocities in the wake as described in section 3. This comparison was made at three advance coefficients and is shown in fig. 5.10. A good correlation was achieved using the two methods for calculating the values of circulation.

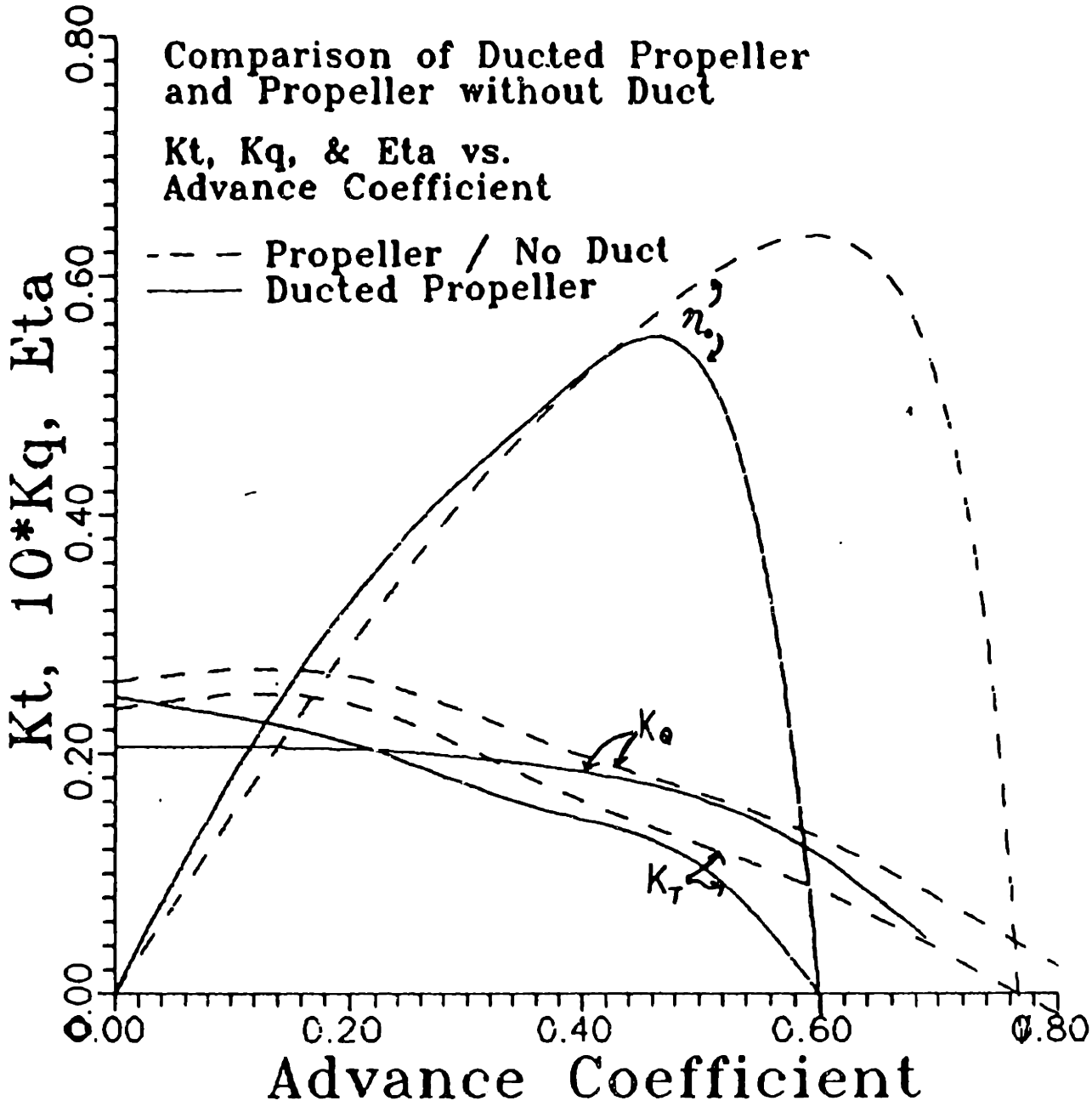

Figure 5.1: Comparison of open and ducted propeller

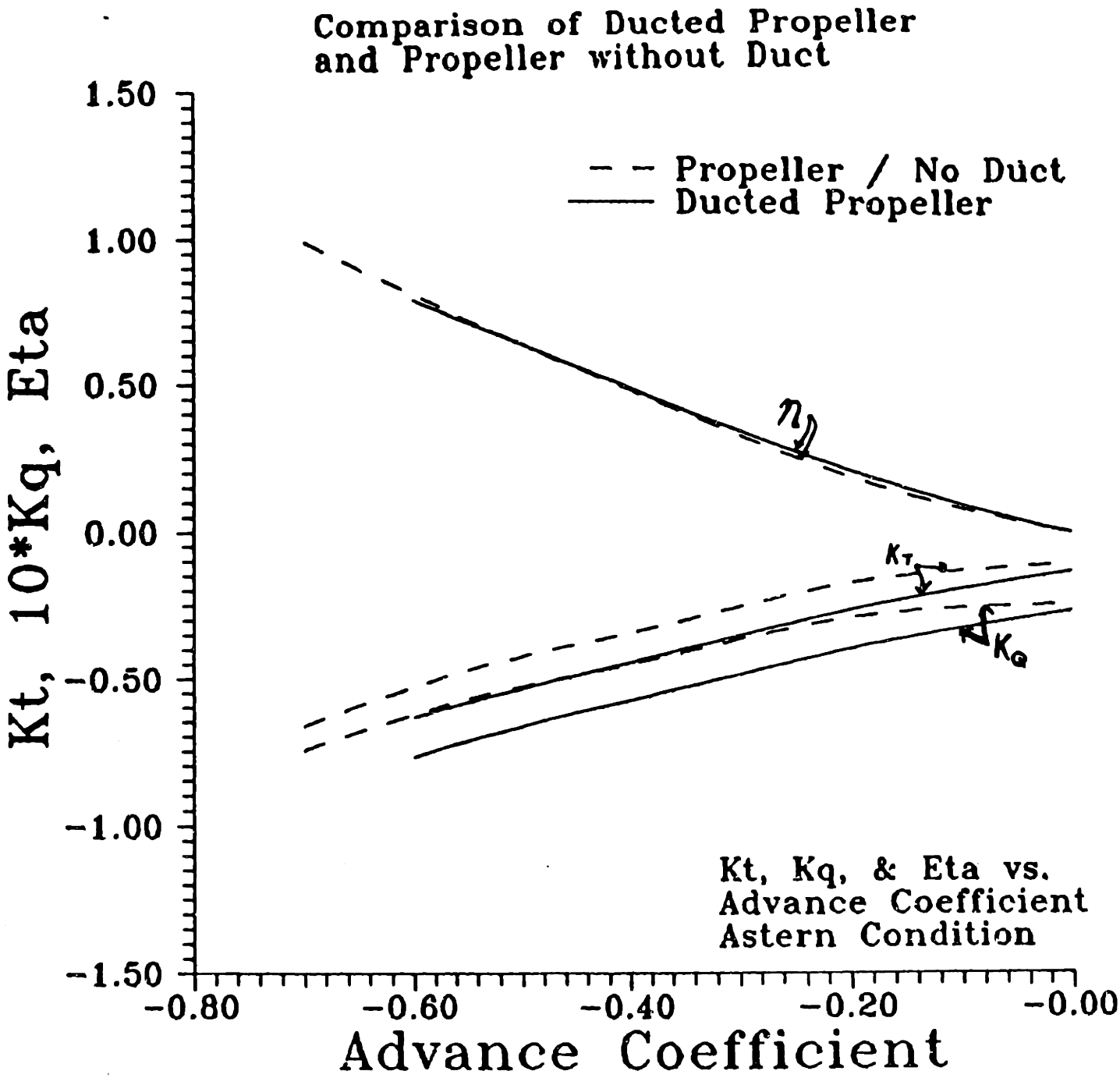

Figure 5.2: Comparison of open and ducted propeller, astern condition

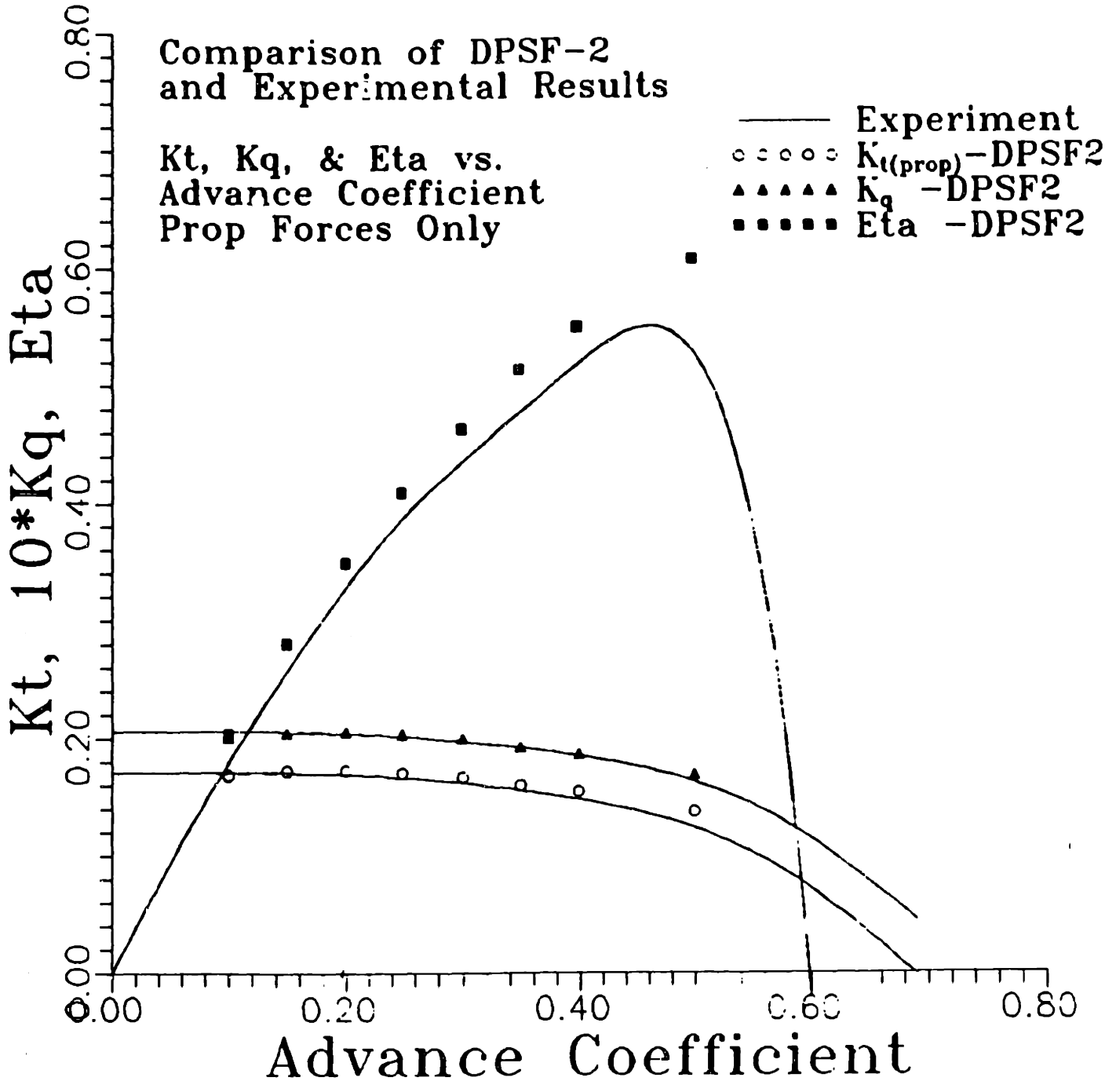

Figure 5.3: Comparison of Experimental and Analytic Forces, Propeller forces only

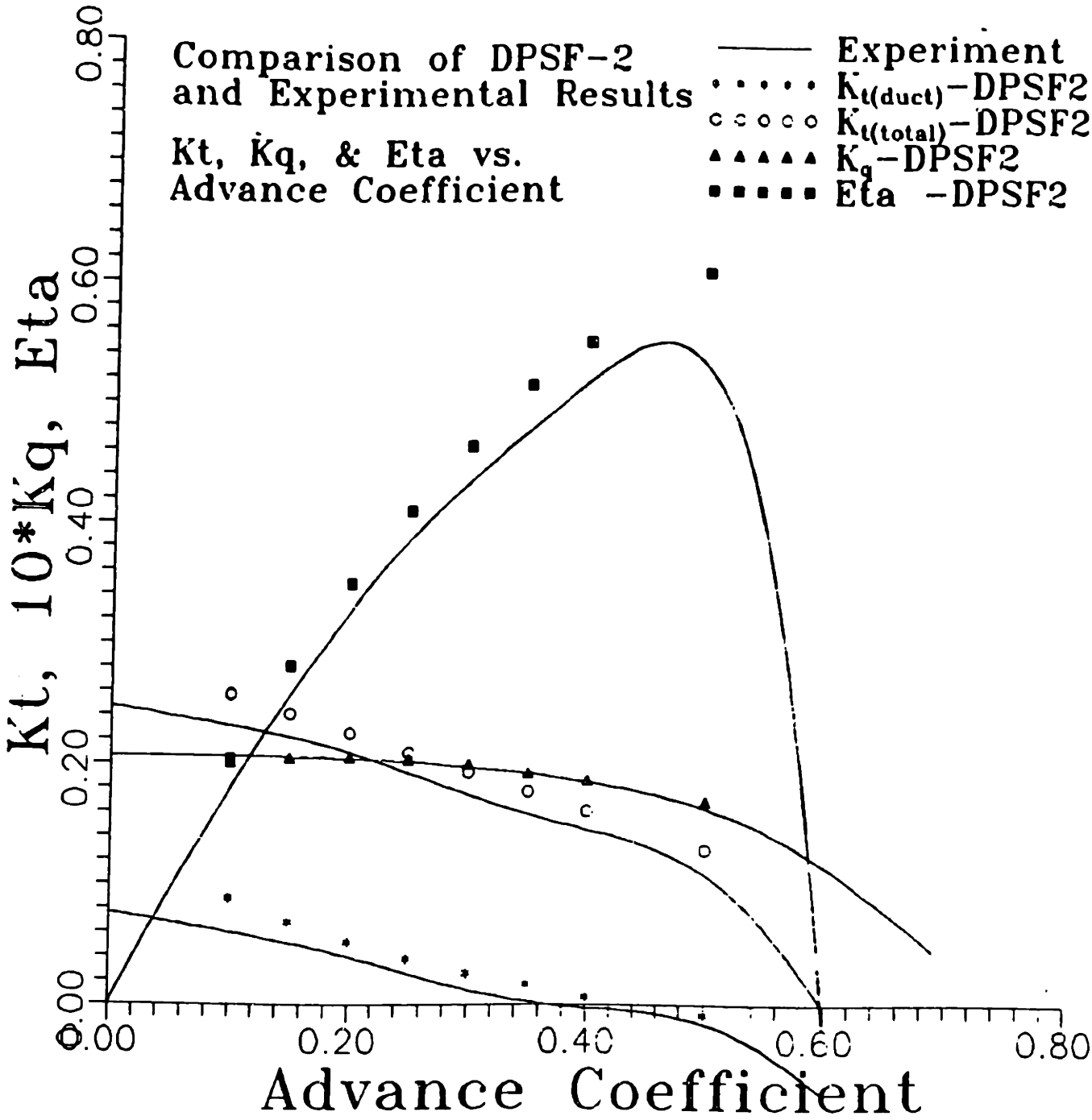

Figure 5.4: Comparison of Experimental and Analytic Forces, Propeller and duct forces

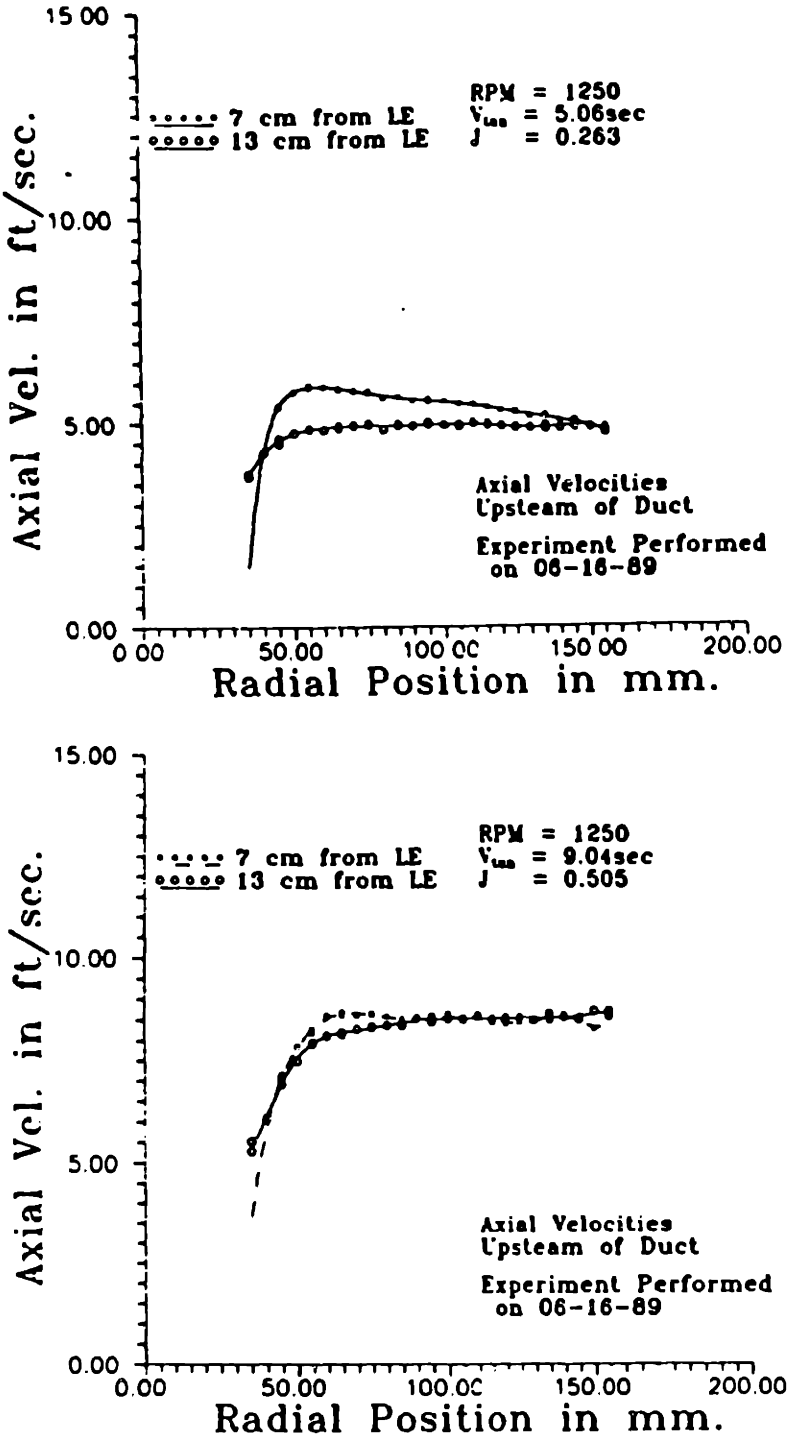

Figure 5.5: Upstream axial velocities

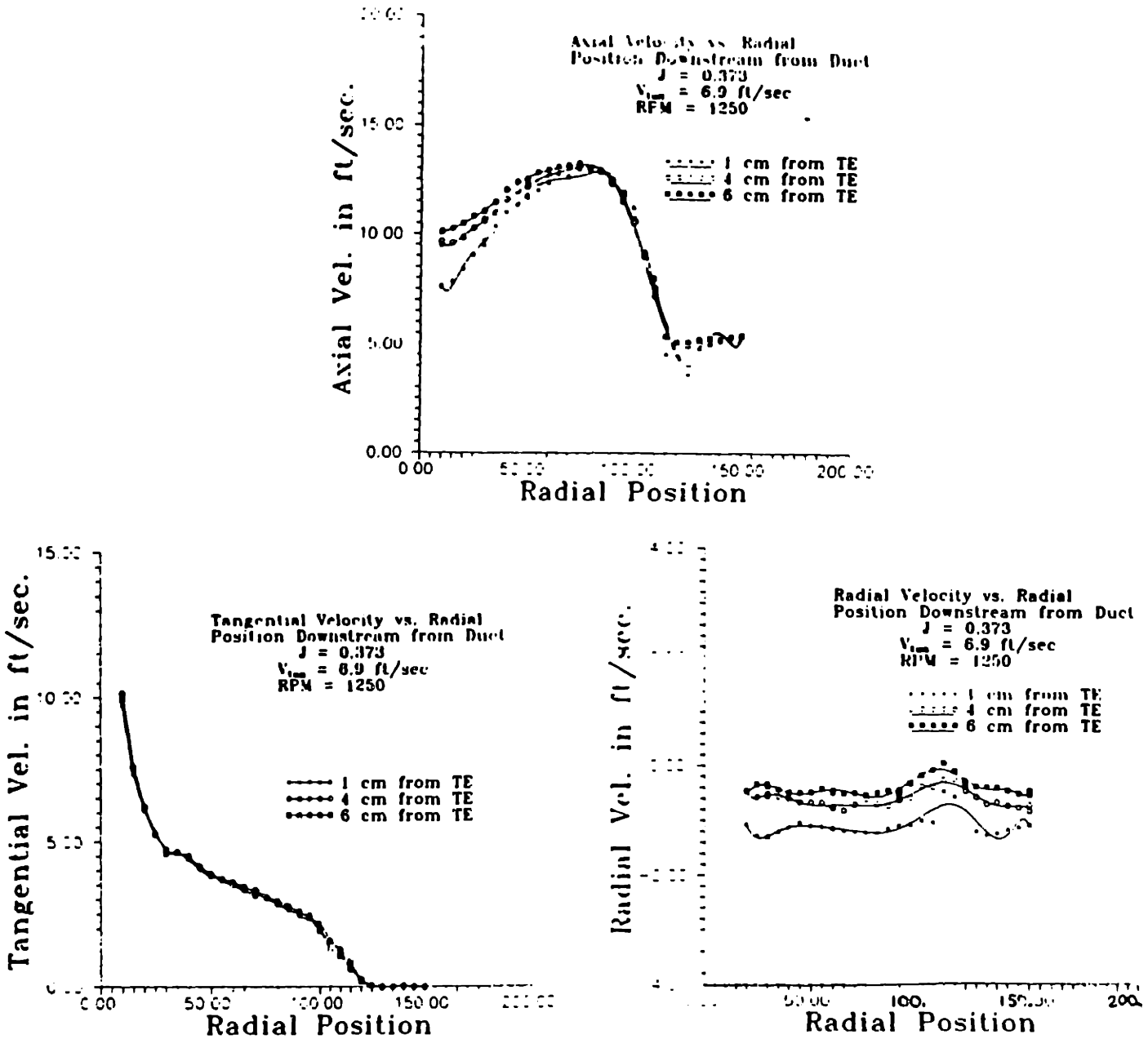

Figure 5.7: Velocities measured aft of duct J=0.373

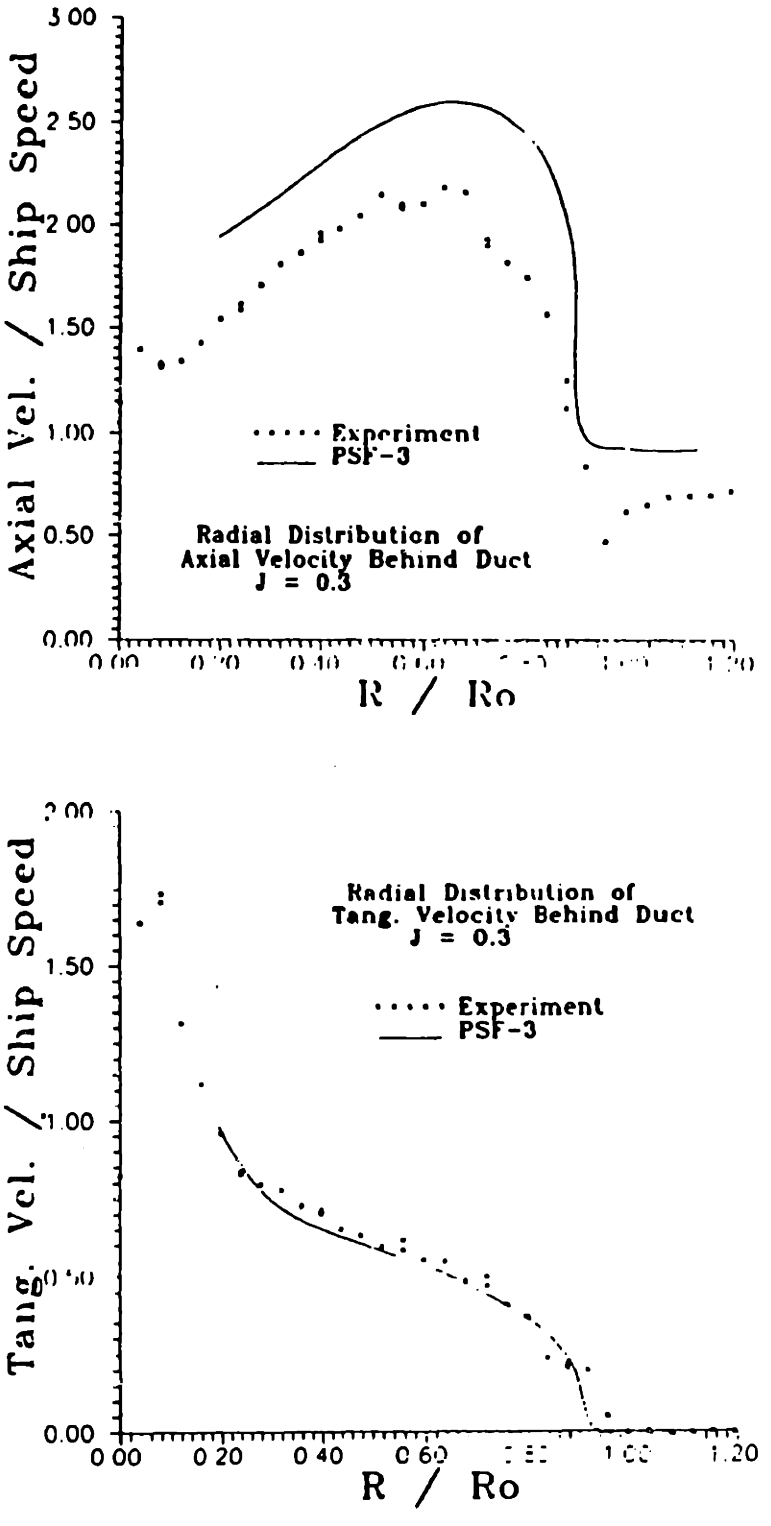

Figure 5.8: Comparison of experimental and analytical velocities, J=0.3

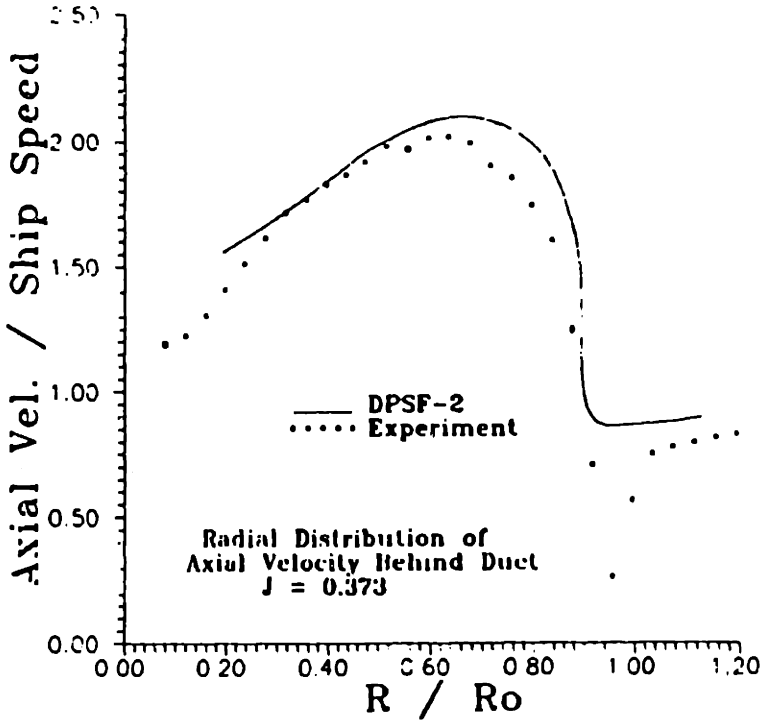

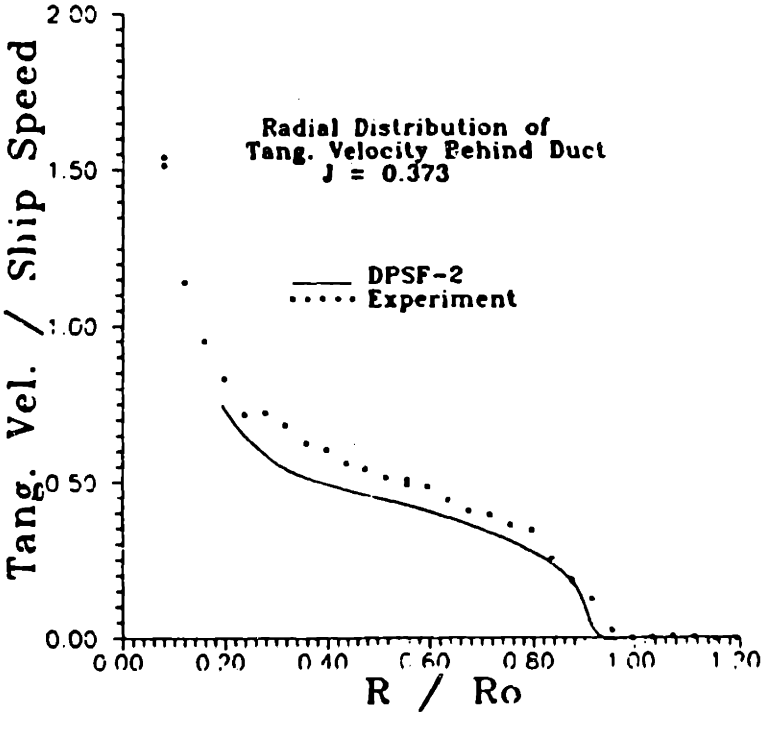

Figure 5.9: Comparison of experimental and analytical velocities, J=0.373

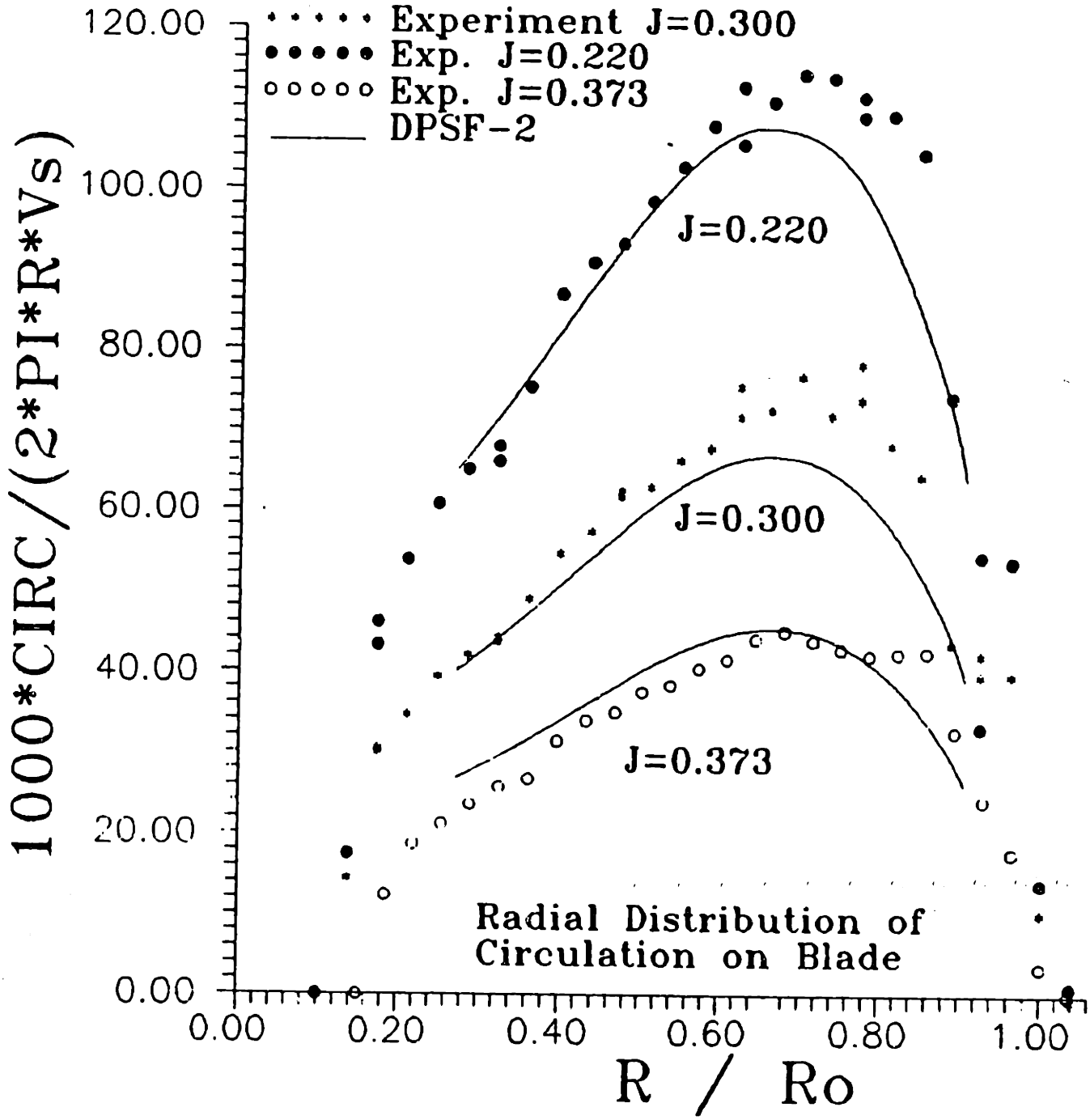

Figure 5.10: Comparison of experimental and analytical distributions for the spanwise distribution of circulation on the propeller.

Chapter 6

Conclusions and Future Research

The following has been accomplished in this thesis:

- A duct was designed to operate efficiently with an existing propeller. Experiments on the ducted propeller were performed in the MIT Variable Pressure Water Tunnel, and the duct appeared to perform as expected.
- The ducted propeller was modelled analytically using the DPSF-2 computer program. Very good agreement over a large range of advance coefficients was shown between the theoretical and experimental values for the forces on the duct and propeller and the circulation on the propeller.
- Velocity measurements were made using the LDV system at the MIT propeller tunnel. The velocity field measured behind the ducted propeller model behaved as expected.
- A method was developed to predict the velocity at any field point in the region surrounding a ducted propeller. The velocities predicted showed reasonable agreement with those measured experimentaly.

As mentioned in the previous chapter, a more accurate prediction of the effect of the tunnel wall on the velocities in the region surrounding a ducted propeller could be

obtained if the tunnel were modelled along with the duct, hub, and propeller within DPSF-2. A method for calculating the effect of the tunnel walls both in uniform and in shear flow was developed by Shih in [12]. The incorperation of this method into DPSF-2 is currently being worked on so that a better comparison to the experimental axial velocities can be made.

My current research concerns the analysis of ducted propellers operating in combination with pre-swirl stator vanes. Since a ducted propeller often requires struts to support the duct, it appears logical to use these supports as a set of pre-swirl stator vanes if a gain in efficiency could be achieved. One possible application is to use a ducted propeller with a set of controllable-pitch pre-swirl stators; in this manner the thrust provided by the ducted propeller could be changed without modifying the motor rpm. The ducted propeller analysis code DPSF-2 has been modified to include the presence of pre-swirl stators. This extended version of the code has been used to design a combination of duct and stators to operate efficiently with an existing propeller using the same procedure that was described in section 2. A preliminary investigation has shown that for this ducted propeller, pre-swirl stators have the potential to increase the efficiency of the system by roughly 5% and can be used to vary the magnitude of the thrust over 50% at a constant rpm and inflow velocity. Tests have been planed for this ducted propeller and stator combination after which more comparisons can be made.

Bibliography

[1] I.S. Gibson and R.I. Lewis. Ducted propeller analysis by surface vorticity and actuator disc theory. In *Proceedings of the Symposium on Ducted Propellers*, The Royal Institution of Naval Architects. Teddington, England, MAY 1973.

[2] H. Glauert. *The Elements of Aerofoil and Airscrew Theory, 2nd Edition.* Cambridge University Press, New York. 1947.

[3] E.J. Glover and P.G. Ryan. A comparison of the theoretical and experimental performance of a ducted propeller system. In *Proceedings of the Symposium on Ducted Propellers*, The Royal Institution of Naval Architects, Teddington, England, MAY 1973.

[4] D.S. Greeley and J.E. Kerwin. Numerical methods for propeller design and analysis in steady flow. *Trans. SNAME*, vol 90, 1982.

[5] J.E. Kerwin, S.A. Kinnas, J-T Lee. and W-Z Shih. A surface panel method for the hydrodynamic analysis of ducted propellers. *Trans. SNAME*, 95, 1987.

[6] S.A. Kinnas. Ducted Propeller Steady Flow, MIT-DPSF2, User's Manual. May 1989. MIT, Department of Ocean Engineering Report.

[7] Spyros A. Kinnas and William B. Coney. On the optimum ducted propeller loading. In *Proceedings of the Propellers '88 Symposium*, SNAME, Virginia Beach, VA, September 1988.

[8] Spyros A. Kinnas and William B. Coney. A systematic method for the design of ducted propellers. In *Proceedings of the Fourth International PRADS89 Symposium*, Varna, October 23-28 1989.

[9] Wang M.H. *Hub Effects in Propeller Design and Analysis.* Technical Report No 85-12, Department of Ocean Engineering, MIT, May 1985.

[10] Luigi Morino and Ching-Chiang Kuo. Subsonic potential aerodynamic for complex configurations : a general theory. *AIAA J.*, vol 12(no 2):pp 191–197, February 1974.

[11] Van Houten R. *Analysis of Ducted Propellers in Steady Flow.* Technical Report 4.76-1, Airflow Research and Manufacturing Corp., Watertown, MA., February 1986.

[12] Wei-Zen Shih. *Effective Wake Calculations by Solving The Euler Equation.* Technical Report No 88-2, Department of Ocean Engineering, MIT, 1988.

Appendix A

Geometry of the Propeller and Duct

TABLE A-1. GEOMETRY OF DTNSRDC PROPELLER 3745

Number of Blades = 5

Parabolic arc camber

NACA-16 thickness form

Diameter = 9.9 inches

R/RO	P/D	RAKE/D	SKEW	C/D	F/C	T/D
0.2000	0.5734	0.0000	0.0000	0.1698	0.0459	0.0416
0.3000	0.6031	0.0000	0.0000	0.2057	0.0380	0.0359
0.4000	0.6317	0.0000	0.0000	0.2359	0.0331	0.0303
0.5000	0.6560	0.0000	0.0000	0.2562	0.0304	0.0248
0.6000	0.6707	0.0000	0.0000	0.2667	0.0284	0.0198
0.7000	0.6764	0.0000	0.0000	0.2667	0.0258	0.0152
0.8000	0.6714	0.0000	0.0000	0.2505	0.0210	0.0109
0.9000	0.6515	0.0000	0.0000	0.2101	0.0147	0.0069
0.9500	0.6296	0.0000	0.0000	0.1719	0.0115	0.0050
1.0000	0.5969	0.0000	0.0000	0.1094	0.0062	0.0030

TABLE A-2. OFFSETS FOR THE DUCT

NOTE: ORIGIN LOCATED AT THE DUCT TRAILING EDGE ON THE PROPELLER AXIS

ALL DIMENSIONS ARE IN INCHES

DUCT INNER SURFACE		DUCT OUTER SURFACE	
X	R	X	R
5.023	6.131	5.023	6.131
5.020	6.099	5.005	6.156
4.993	6.064	4.944	6.183
4.944	6.027	4.845	6.200
4.873	5.986	4.747	6.206
4.780	5.942	4.628	6.206
4.626	5.876	4.491	6.200
4.488	5.822	4.335	6.189
4.333	5.746	4.103	6.164
4.162	5.702	3.912	6.138
3.976	5.638	3.708	6.105
3.778	5.572	3.494	6.067
3.568	5.505	3.272	6.024
3.349	5.436	3.120	5.992
3.123	5.367	2.887	5.940
2.891	5.300	2.573	5.860
2.656	5.236	2.338	5.791

2.418	5.157	2.105	5.716
2.181	5.119	1.802	5.608
1.870	5.050	1.582	5.523
1.568	4.989	1.303	5.407
1.281	4.935	1.106	5.322
1.014	4.888	0.920	5.238
0.830	4.857	0.749	5.158
0.608	4.822	0.544	5.060
0.462	4.799	0.409	4.993
0.334	4.780	0.258	4.917
0.227	4.764	0.166	4.870
0.116	4.749	0.094	4.833
0.059	4.740	0.042	4.806
0.025	4.736	0.010	4.790
0.000	4.732	0.000	4.784

DUCT TRAILING EDGE THICKNESS

(STRAIGHT LINE SEGMENT)

X	R
0.000	4.784
0.000	4.732

Appendix B

Computation of Velocity Field

The velocity is first computed with respect to a coordinate system which rotates with the propeller. In order to tranform this velocity back to a fixed set of axies, the rotational velocity of the propeller system $\vec{\omega} \times \vec{r}$ must be subtacted from the computed velocity. The velocity calculated at a given field point is actually the sum of three velocity components:

$$\vec{V} = \vec{V}_{in} + \vec{V}_{prop} + \vec{V}_{duct}$$

where:

- $\vec{V}_{in}$ is the inflow velocity distribution which is the given free stream velocity distribution plus the rotational speed of the coordinate system, $\vec{\omega} \times \vec{r}$.
- $\vec{V}_{prop}$ is the propeller induced velocity.
- $\vec{V}_{duct}$ is the duct and hub induced velocity.

The method for calculating the last two velocity components will be discussed separately below. Note that this method calculates the non-axisymmetric velocity at a field point with a specified axial, radial, and angular position with respect to the propeller. This can then be used at a series of points to calculate the circumferentially averaged velocity as described in the text.

Duct Induced Velocities

The duct and hub are represented using a potential based panel method. The procedure used for calculating the velocity using this method is described briefly here. Consider a volume bounded by the surface of the duct, S_D; the duct wake, S_W; and an outer control surface, S_∞. The duct is assumed to be operating in an incompressible irrotational, inviscid fluid. Therefore, the velocity field can be expressed in terms of the perturbation velocity potential, ϕ, which must satisfy Laplace's equation and the inflow velocity defined above, $\vec{V}_{in}$.

$$\vec{V} = \nabla\phi + \vec{V}_{in}$$

$$\nabla^2\phi = 0$$

where:

- ϕ is the perturbation velocity potential.

By making the following definitions:

- ϕ_{duct} is the value of the perturbation potential on the duct surface.
- ϕ_{prop} is the induced perturbation potential due to the propeller.

The boundary value problem on the duct can be formulated as follows:

- The kinematic boundary condition must be satisfied on the body surface, S_D

$$\frac{\partial\phi_{duct}}{\partial n} = -\vec{V}_{in} \cdot \vec{n}$$

- The wake surface has zero thickness; the normal velocity jump and pressure jump across S_W are zero. A jump in potential is allowed.

$$(\Delta p)_{on S_W} = p^+ - p^- = 0$$

$$\left(\Delta\frac{\partial\phi_{duct}}{\partial n}\right)_{S_W} = \left(\frac{\partial\phi_{duct}}{\partial n}\right)^{+} - \left(\frac{\partial\phi_{duct}}{\partial n}\right)^{-} = 0$$

- A Kutta condition is required at the trailing edge of the duct. This states that the flow velocity at the trailing edge of the duct remains finite.

$$|\nabla\phi_{duct}|_{TE} < \infty$$

According to Morino [10], this is equivalent to requiring the jump in potential across the wake surface to be equal to the jump in potential between the upper and lower panels at the duct trailing edge. For a steady lifting problem this is equal to the circulation around the duct.

$$(\Delta\phi)_{on S_W} = \phi^{+}_{duct} - \phi^{-}_{duct} = \Gamma$$

- The velocity induced by the duct and propeller should vanish on the outer surface as the surface moves an infinite distance from the duct.

$$\nabla\phi \rightarrow 0 \; as \; S_\infty \rightarrow \infty$$

According to [7] the perturbation potential on the duct surface can be found by applying Green's theorem on the duct surface:

$$\begin{aligned} 2\pi o_{duct} \;=\; & \int\int_{S_D}\left[\phi_{duct}(q)\frac{\partial}{\partial n_q}\frac{1}{R(p,q)} - \frac{\partial\phi_{duct}}{\partial n_q}\frac{1}{R(p,q)}\right]ds \\ & + \int\int_{S_W}\Delta\phi_{duct}(q)\frac{\partial}{\partial n_q}\frac{1}{R(p,q)}ds + 4\pi\phi_{prop} \end{aligned}$$

where:

- p is the field point
- q is any point on the duct surface S_D or the duct wake surface S_W.

- $R(p,q)$ is the distance between the points p and q and actually corresponds to the infinite fluid domain Green's function.

- Δo_{duct} is the jump in the potential in the wake of the duct.

From this equation the perturbation potential due to the duct can be expressed in terms of source and dipole distributions on the duct and wake surfaces. A numerical solution to this equation can be obtained by approximating the duct surface and the duct wake with planar panels as was shown in fig. 4.1. The dipole and source distribution on each panel is approximated by a constant strength distribution. The strength of the sources is known from the kinematic boundary condition on the duct surface, and the strength of the dipoles in the wake is set equal to the difference in potential of the panels on the upper and lower side of the duct trailing edge. A discretized form of the equation is then applied at control points located at the center of each panel, resulting in a set of linear equations which can then be solved for the unknown dipole strengths, i.e. the potentials. A more complete description of the numerical implementation of the method is discussed in [5].

Away from the duct, the expression for for the perturbation potential at a field point p becomes:

$$\begin{aligned} 4\pi\phi &= \int\int_{S_D} \left[\phi_{duct}(q) \frac{\partial}{\partial n_q} \frac{1}{R(p,q)} - \frac{\partial \phi_{duct}}{\partial n_q} \frac{1}{R(p,q)} \right] ds \\ &\quad + \int\int_{S_W} \Delta\phi_{duct}(q) \frac{\partial}{\partial n_q} \frac{1}{R(p,q)} ds + 4\pi\phi_{prop} \end{aligned}$$

The gradient of the above equation will yield the perturbation velocity induced at a given field point.

$$\begin{aligned} 4\pi\vec{V} &= \int\int_{S_D} \vec{n} \cdot \nabla\phi \nabla_p \left(\frac{-1}{R(p,q)} \right) - \phi \nabla_p \left(\vec{n} \cdot \nabla \left(\frac{1}{R(p,q)} \right) \right) ds \\ &\quad - \int\int_{S_W} \Delta\phi \nabla_p \left(\vec{n} \cdot \nabla \left(\frac{1}{R(p,q)} \right) \right) ds + 4\pi \nabla_p \phi_{prop} \end{aligned}$$

The last term in the equation represents the propeller induced velocity which is determined using the method described in the next section. The first term in the first integral represents the velocity induced by the source distribution on the duct surface, and the second term in the first integral represents the velocity induced by the dipole distribution on the duct surface. The second integral gives the induced velocity from the dipole distribution on the panels in the duct wake. The duct induced velocity at any given field point can then be determined by summing the induced velocities due to the dipole and source panels on the duct and the dipole panels in the duct wake. It is very important that all of the field points are located at least one half of a panel length away from the duct and duct wake panels; otherwize, a large discretization error will be produced.

Propeller Induced Velocities

The procedure for calculating the induced velocity from the propeller is well documented in [4], and only a brief discussion will be given here. The propeller is represented by a set of discrete straight line vortex elements as is shown in fig. 4.1. The velocity induced by a single straight vortex segment of strength Γ at a point p is always perpendicular to the plane containing the point and the vortex segment. The strength of the induced velocity is given by:

$$V = \frac{\Gamma}{4\pi r}[\cos\theta_1 + \cos\theta_2]$$

where:

- r is the perpendicular distance between the field point and the vortex segment.
- θ_1 is the angle formed by the vortex segment and the line connecting the field point to the end of the vortex segment.

- θ_2 is the angle formed by the vortex segment and the line connecting the field point to the other end of the vortex segment.

The total propeller induced velocity is then the sum of the induced velocities due to each vortex segment making up the propeller and its wake. It is important to choose field points which do not fall to close to any of the vortex elements, as this will produce a large discretization error.

Appendix C

Radial and Chordwise Distribution of Loading on the Propeller

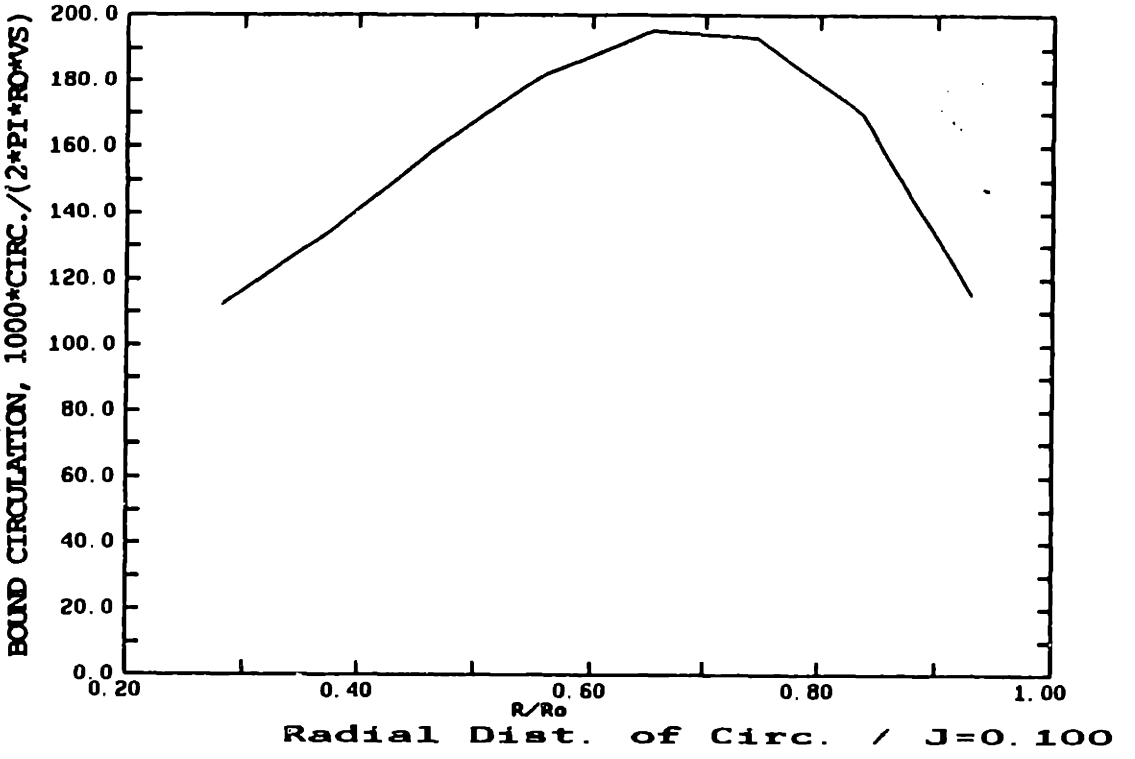

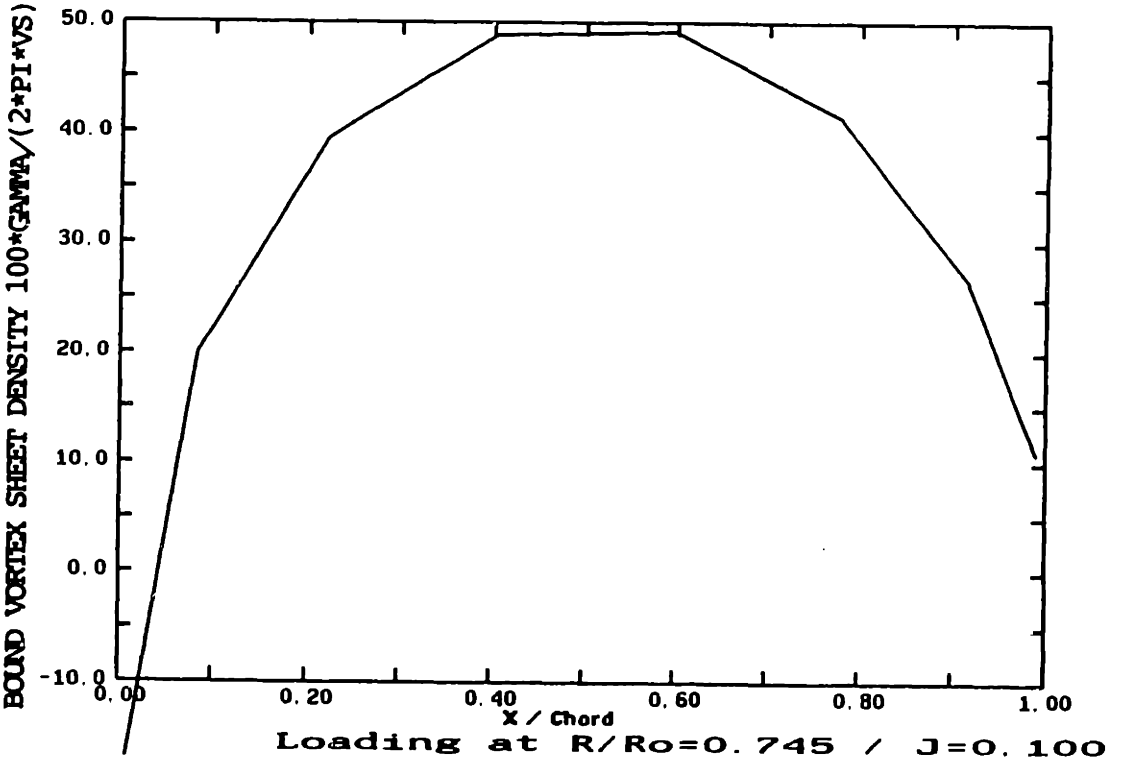

Figure C.1: Radial and chordwise distribution of loading for J=0.100

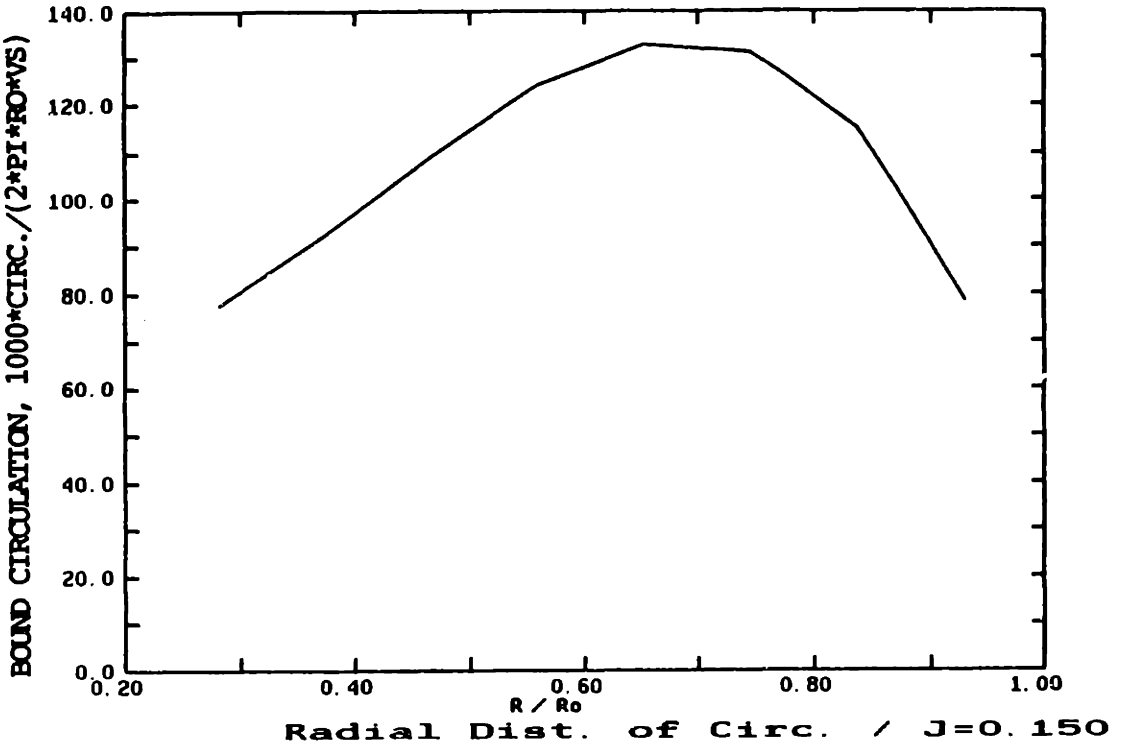

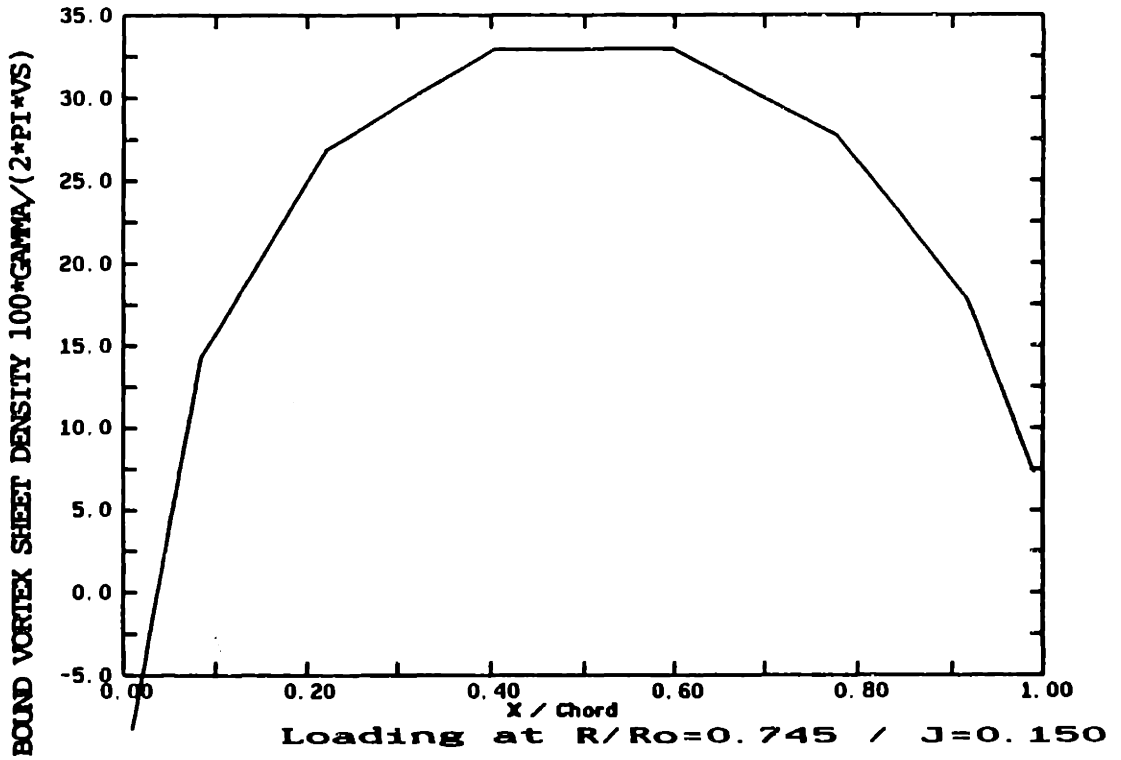

Figure C.2: Radial and chordwise distribution of loading for J=0.150

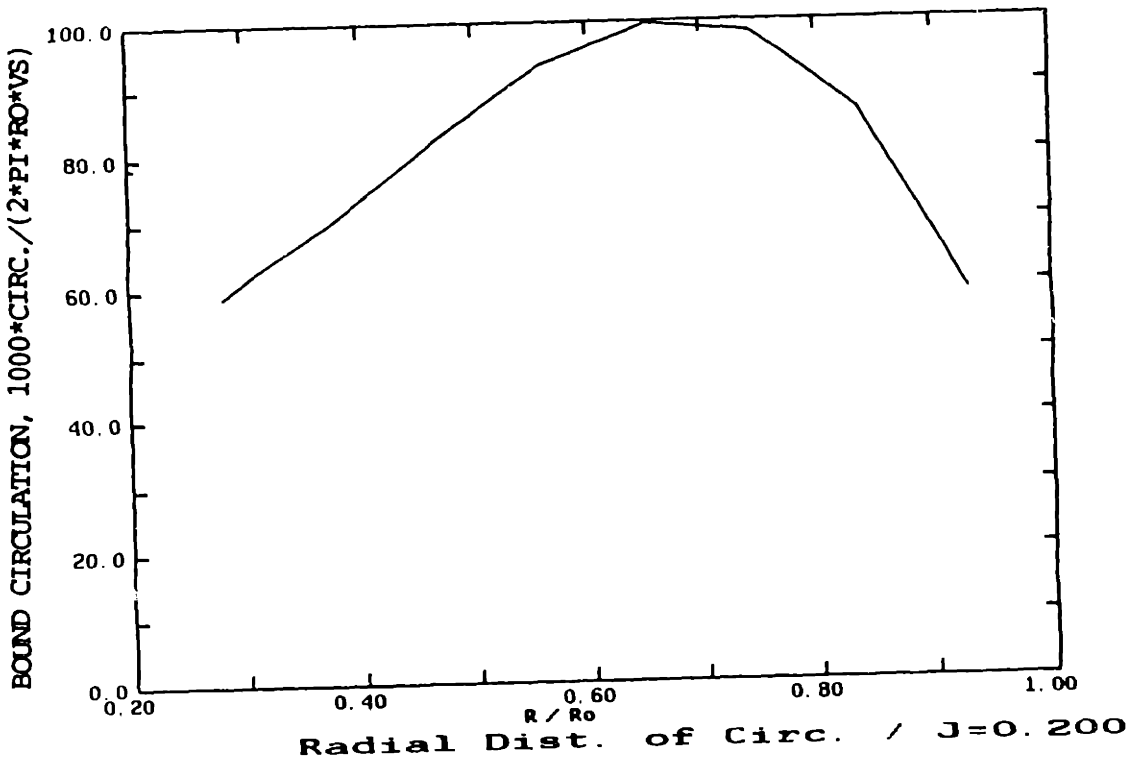

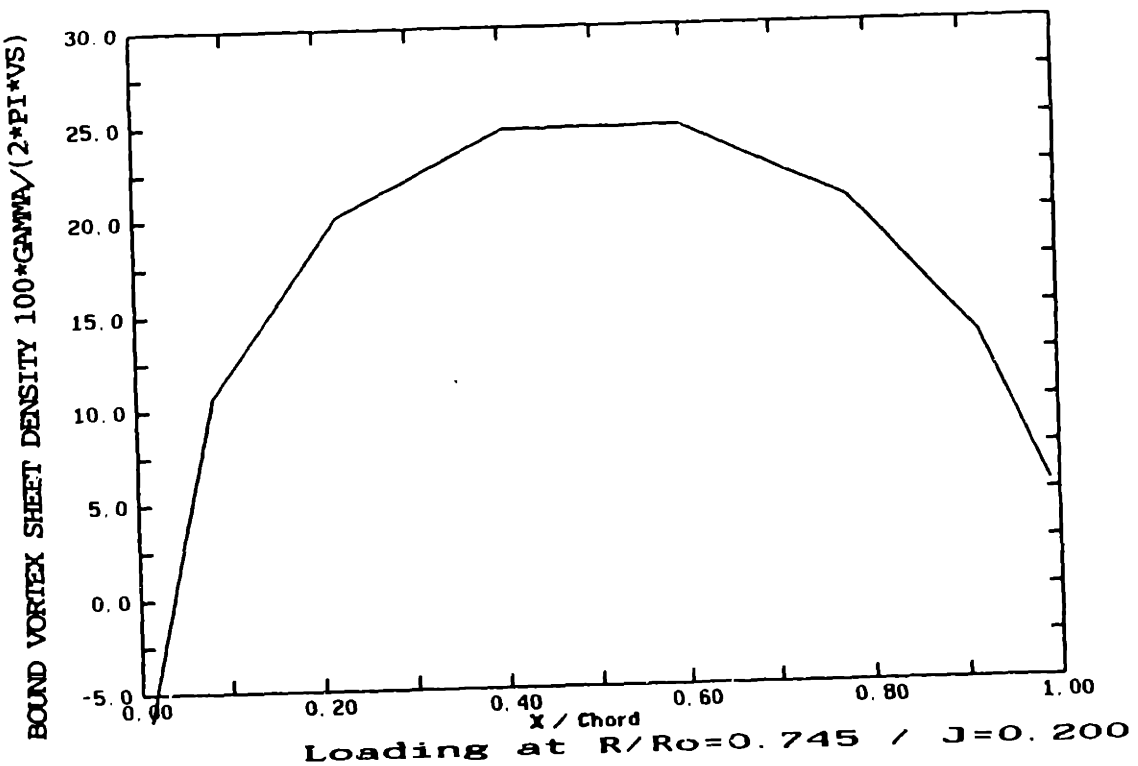

Figure C.3: Radial and chordwise distribution of loading for J=0.200

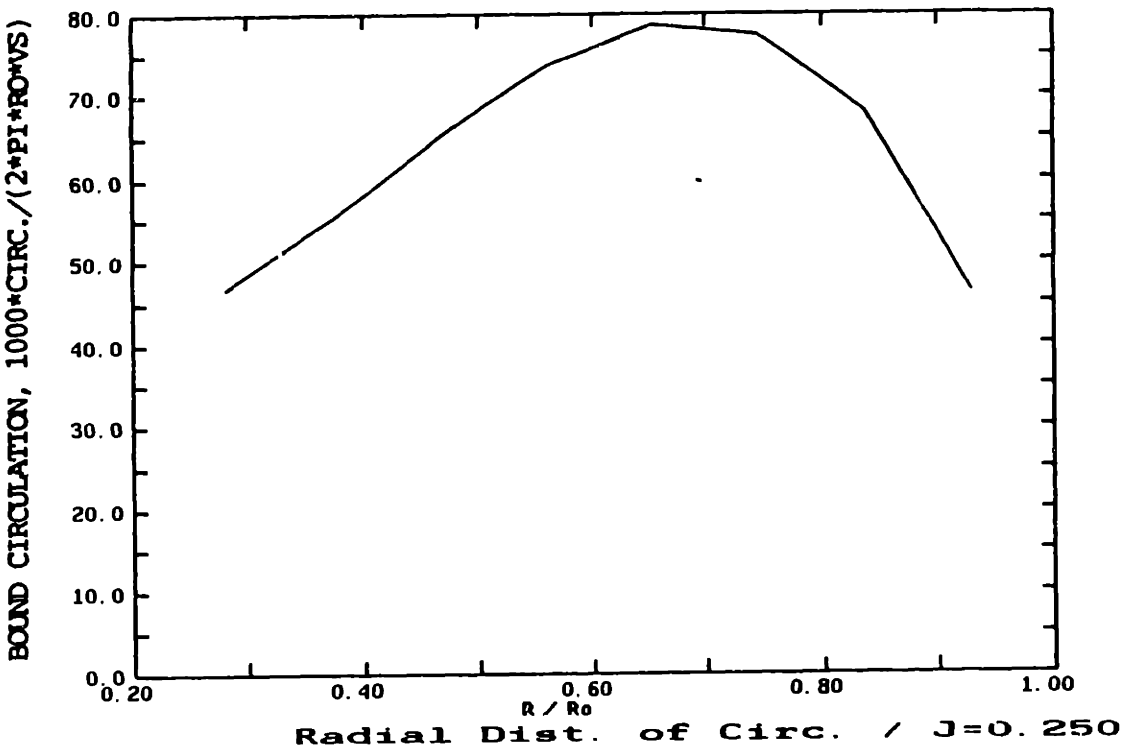

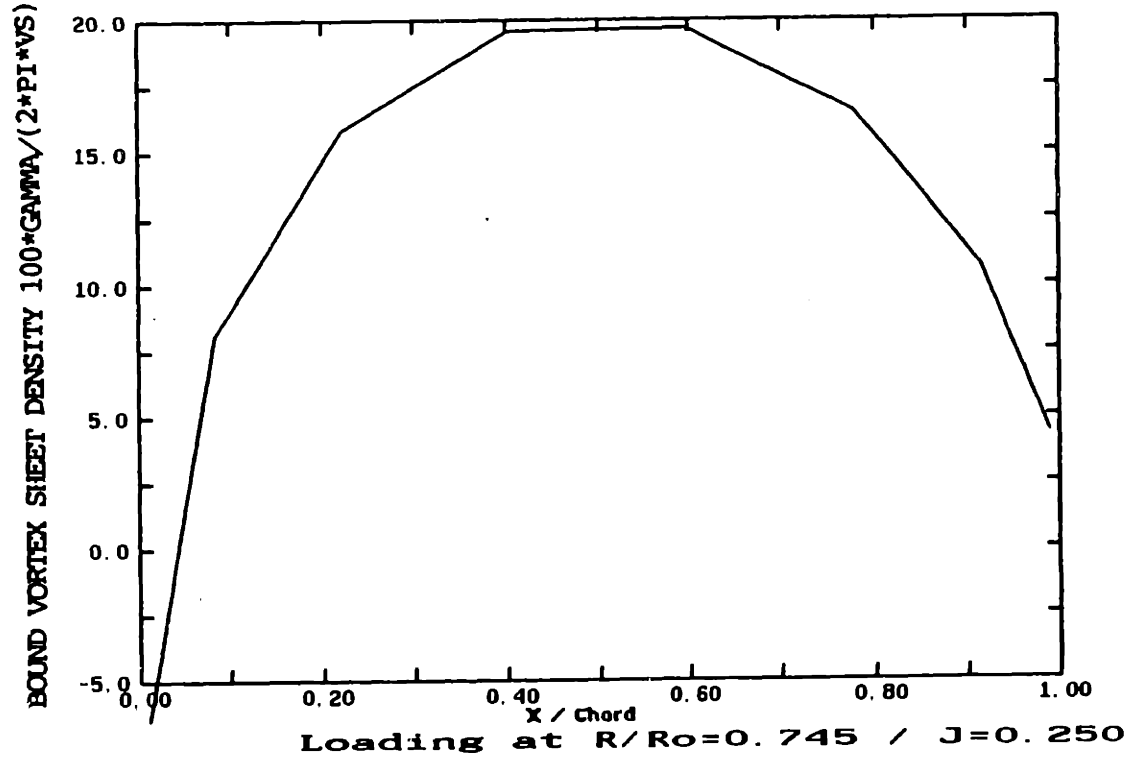

Figure C.4: Radial and chordwise distribution of loading for J=0.250

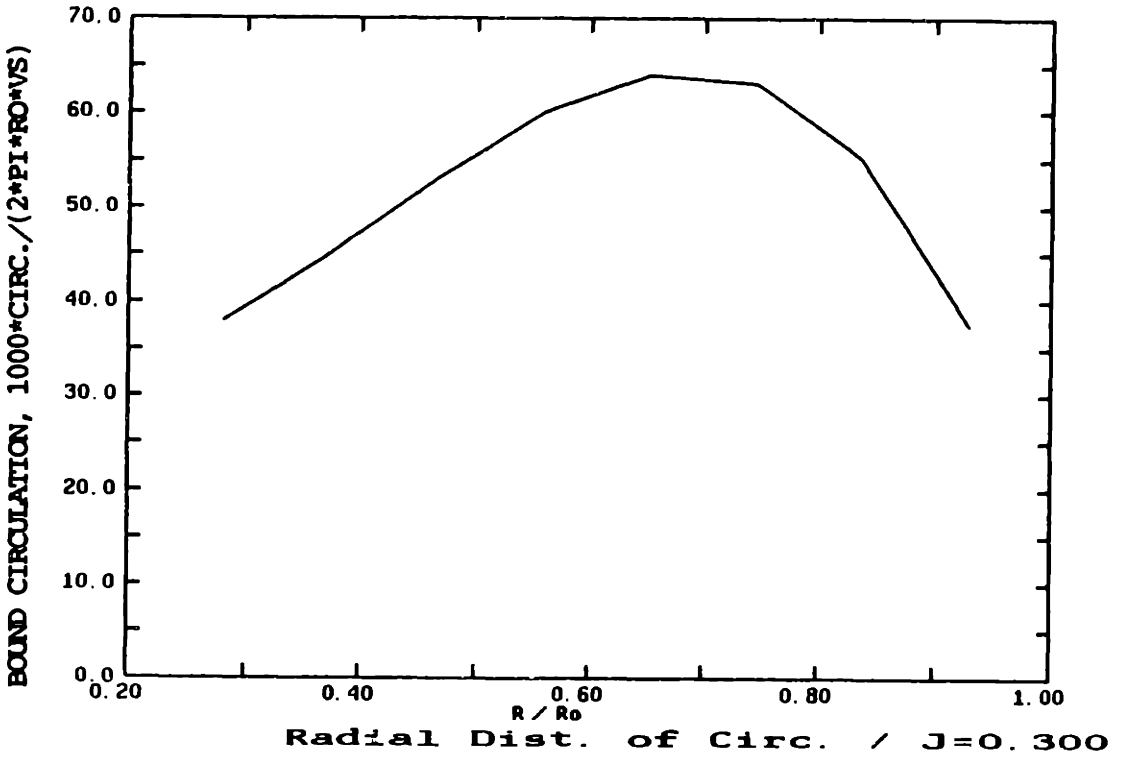

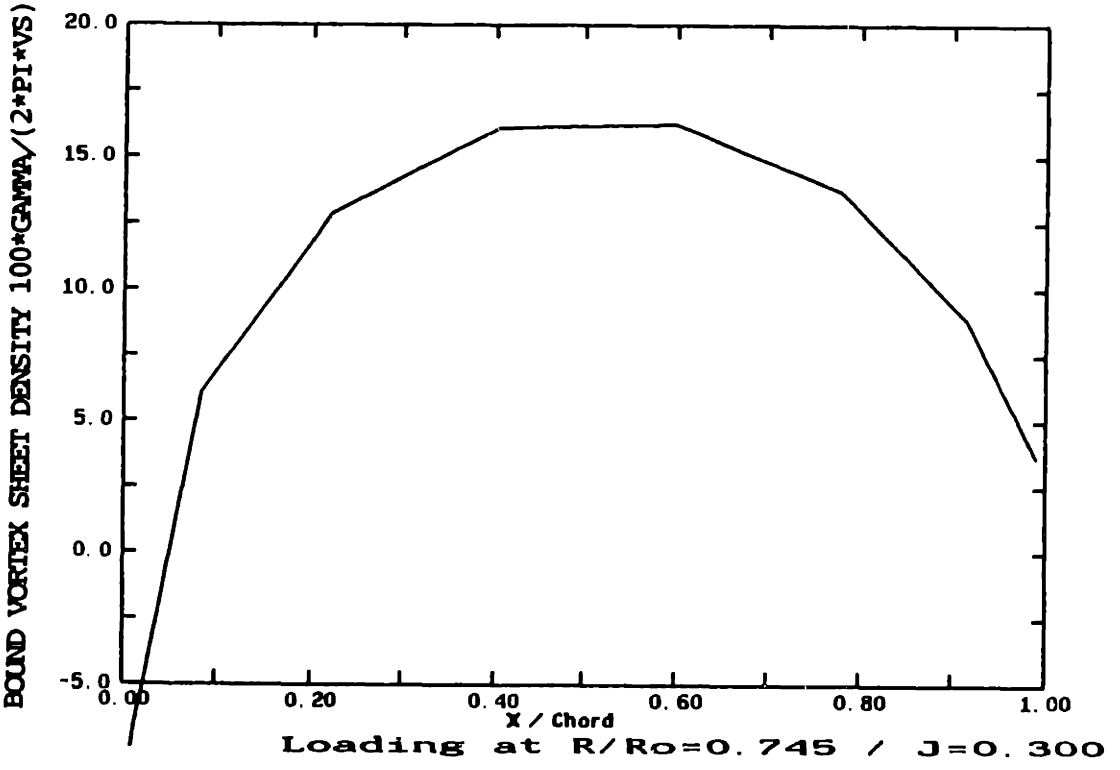

Figure C.5: Radial and chordwise distribution of loading for J=0.300

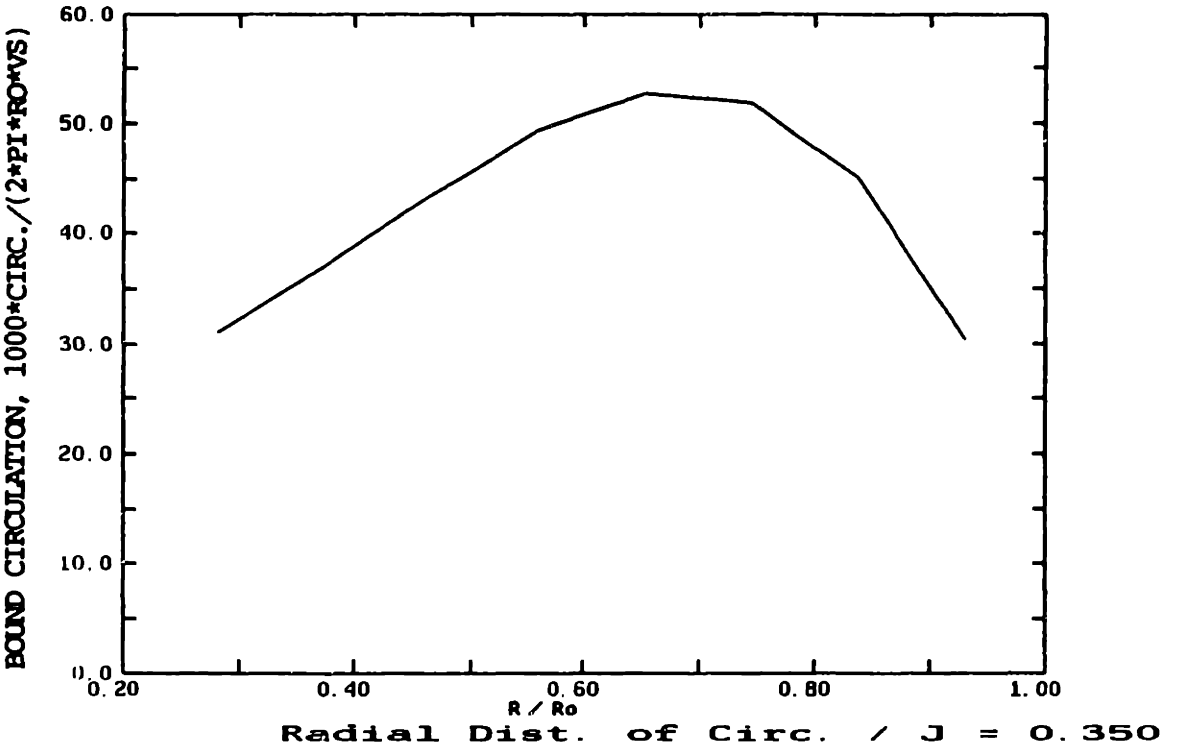

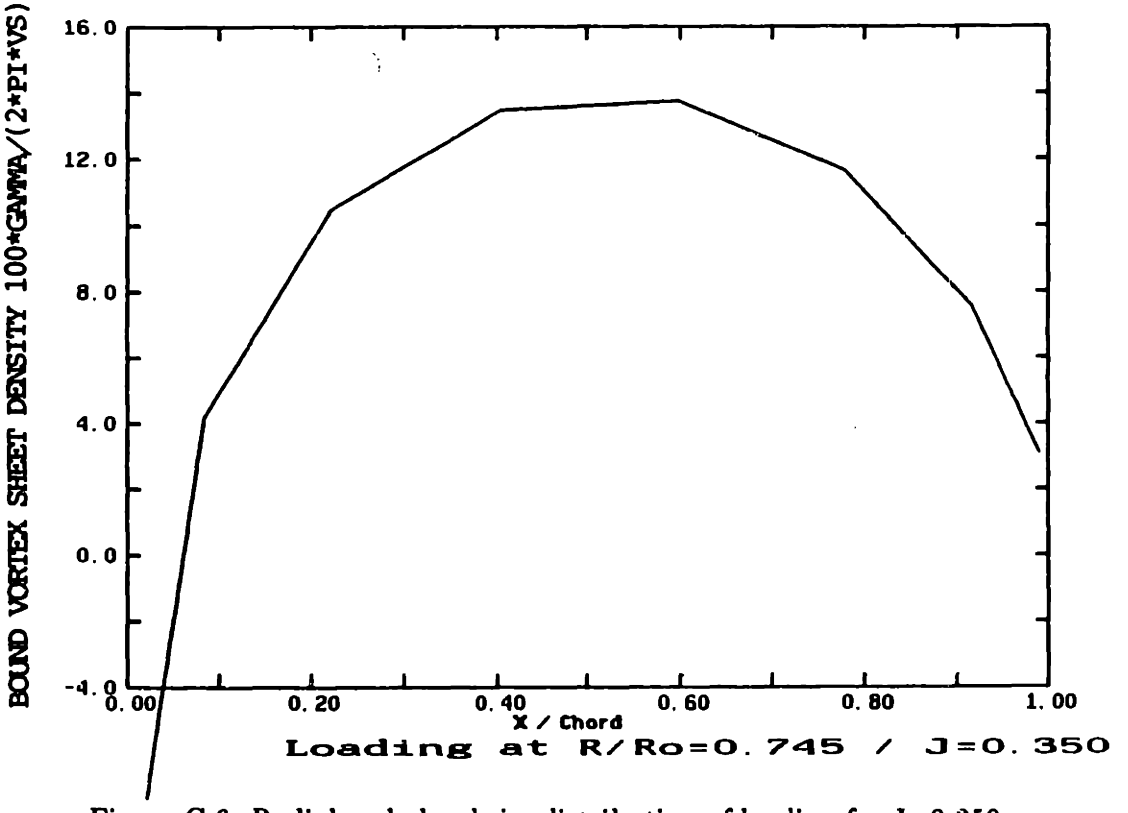

Figure C.6: Radial and chordwise distribution of loading for J=0.350

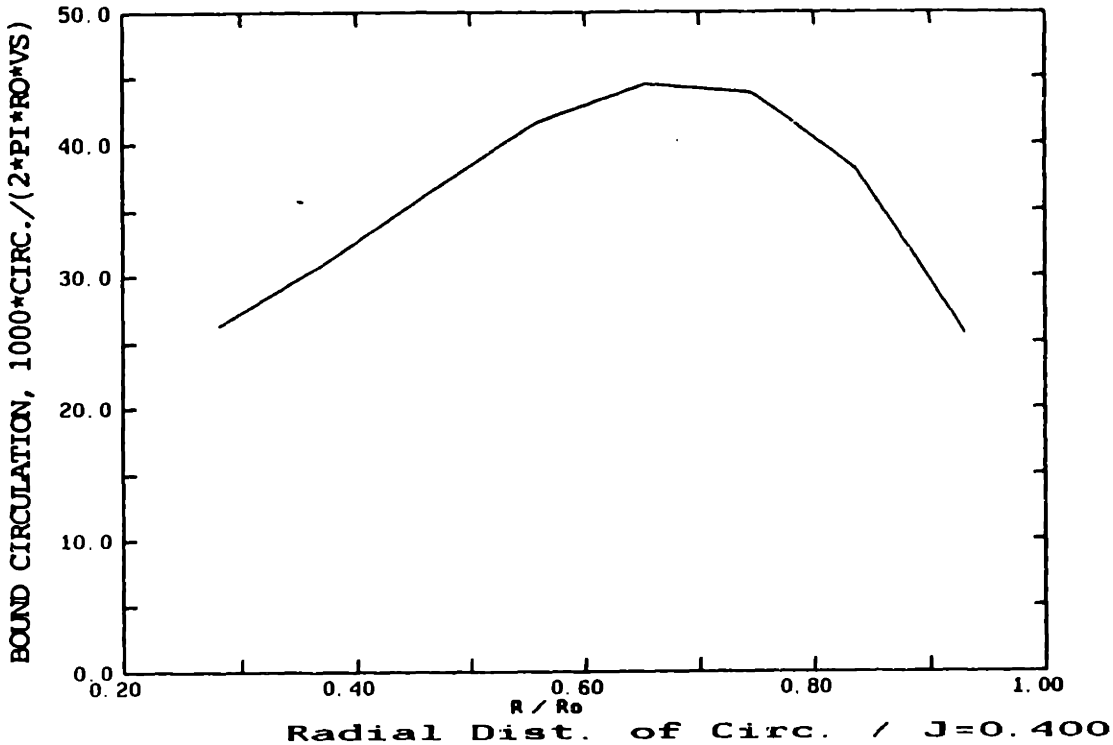

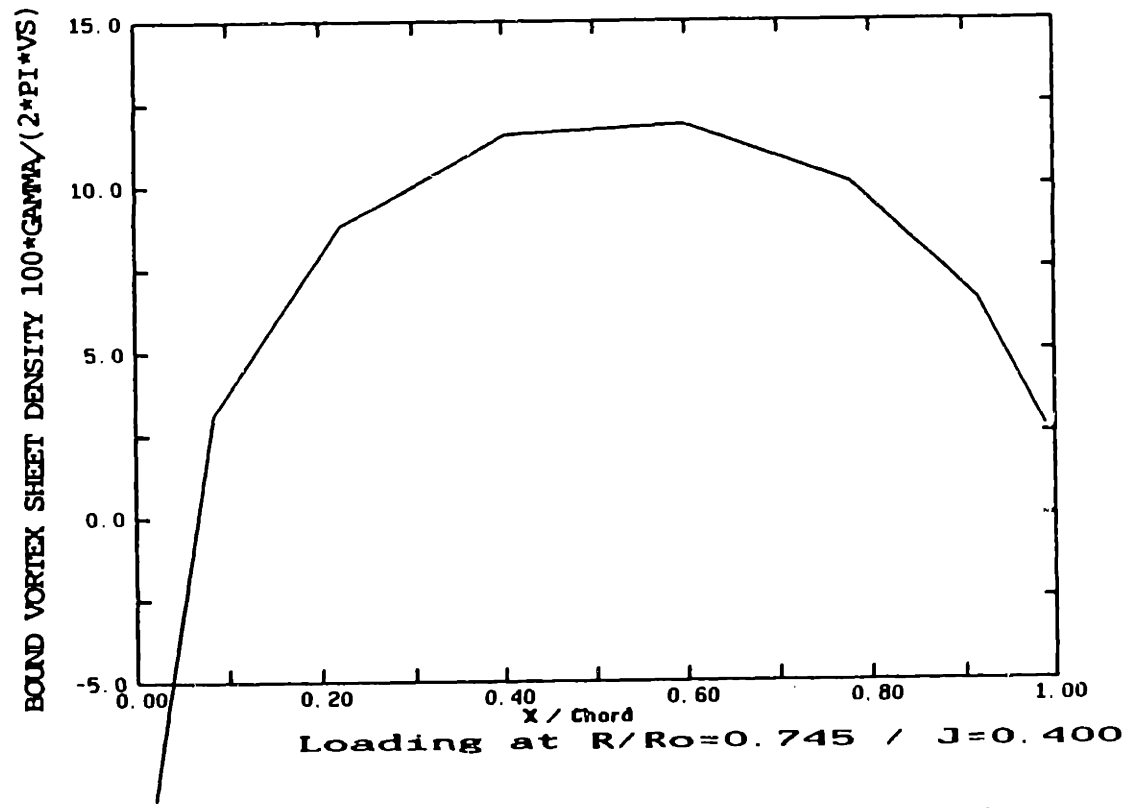

Figure C.7: Radial and chordwise distribution of loading for J=0.400

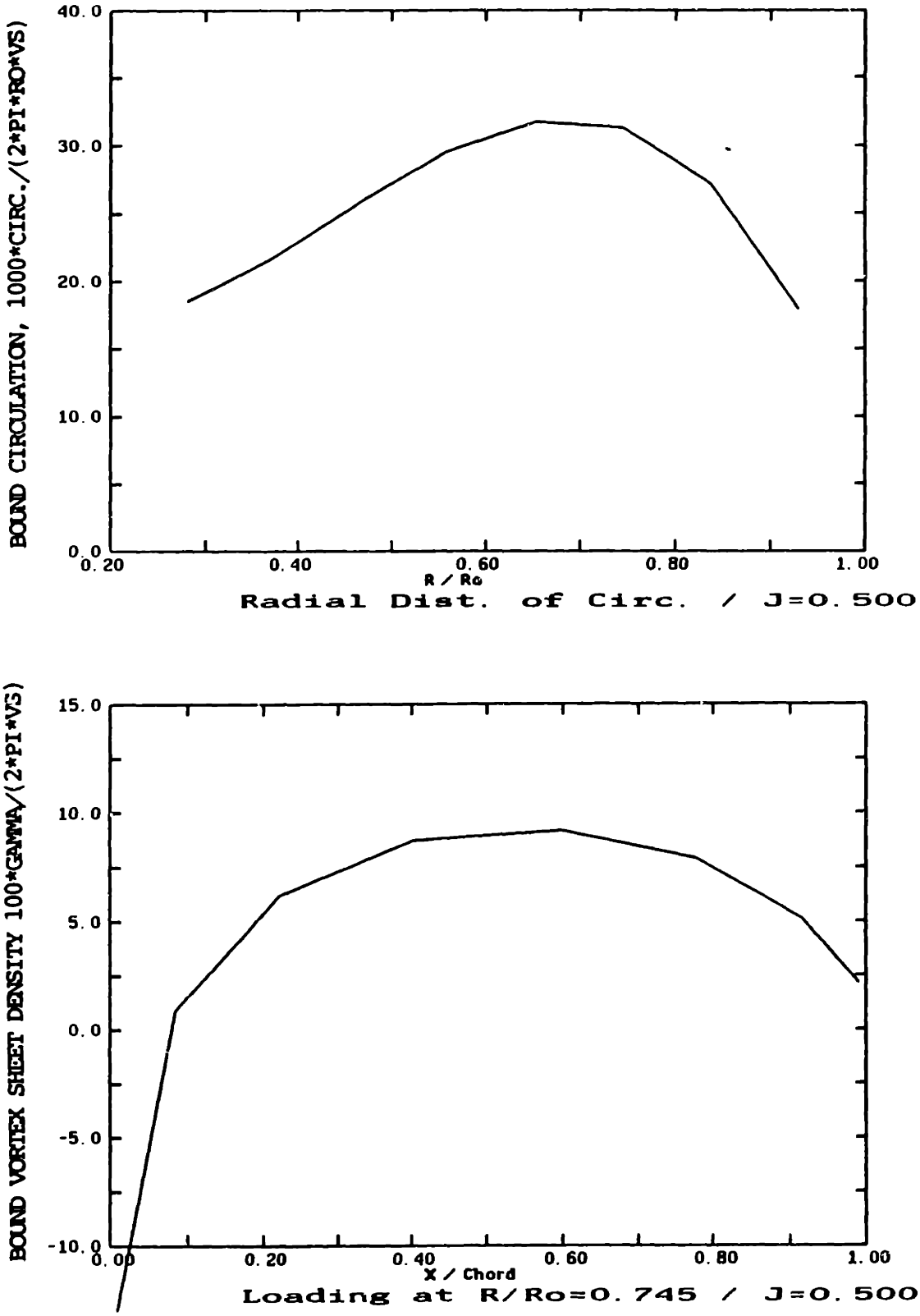

Figure C.8: Radial and chordwise distribution of loading for J=0.500

Appendix D

Distribution of Pressure on the Duct

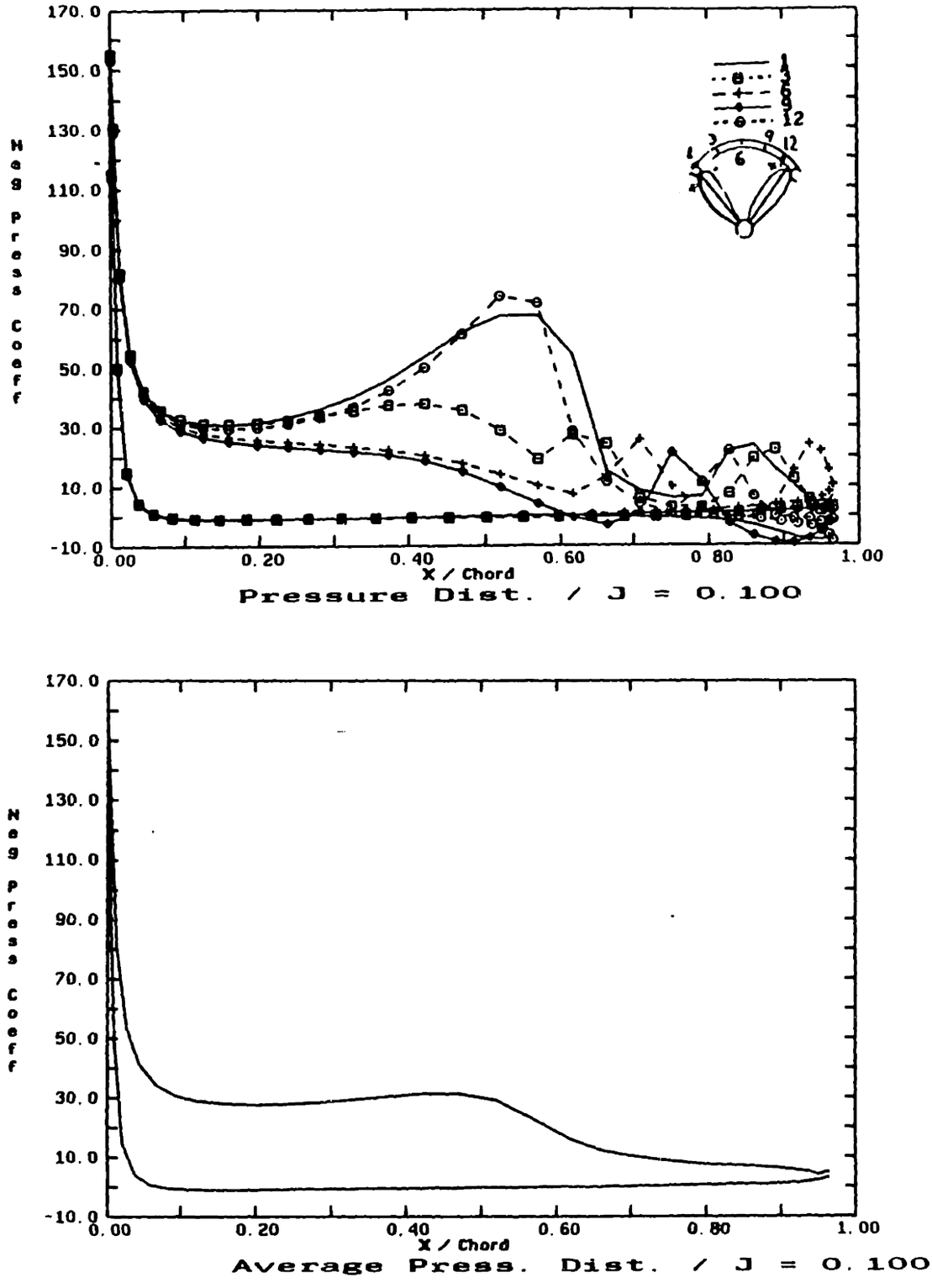

Figure D.1: Duct pressure distribution for J=0.100

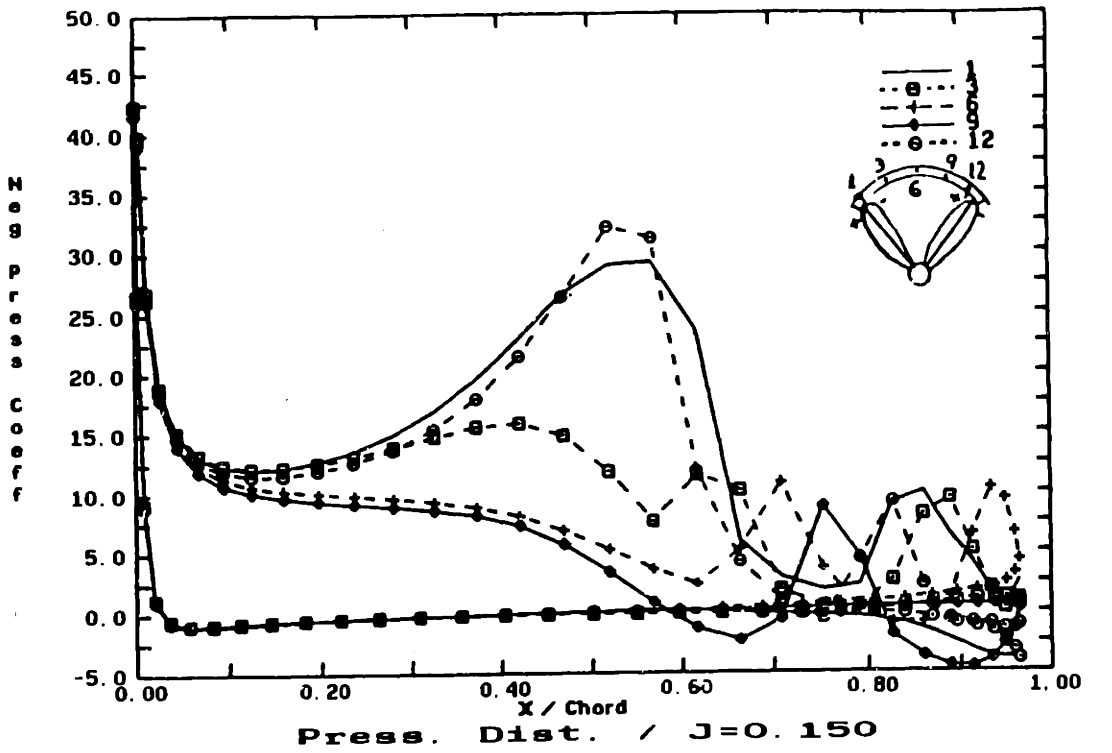

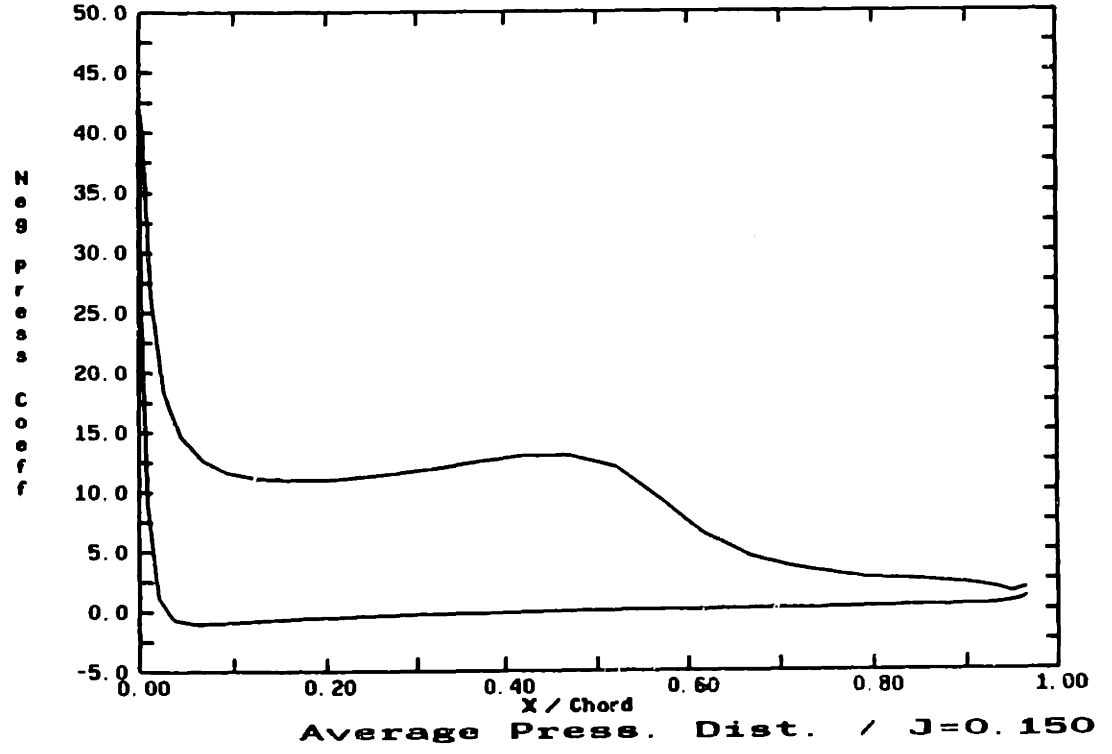

Figure D.2: Duct pressure distribution for J=0.150

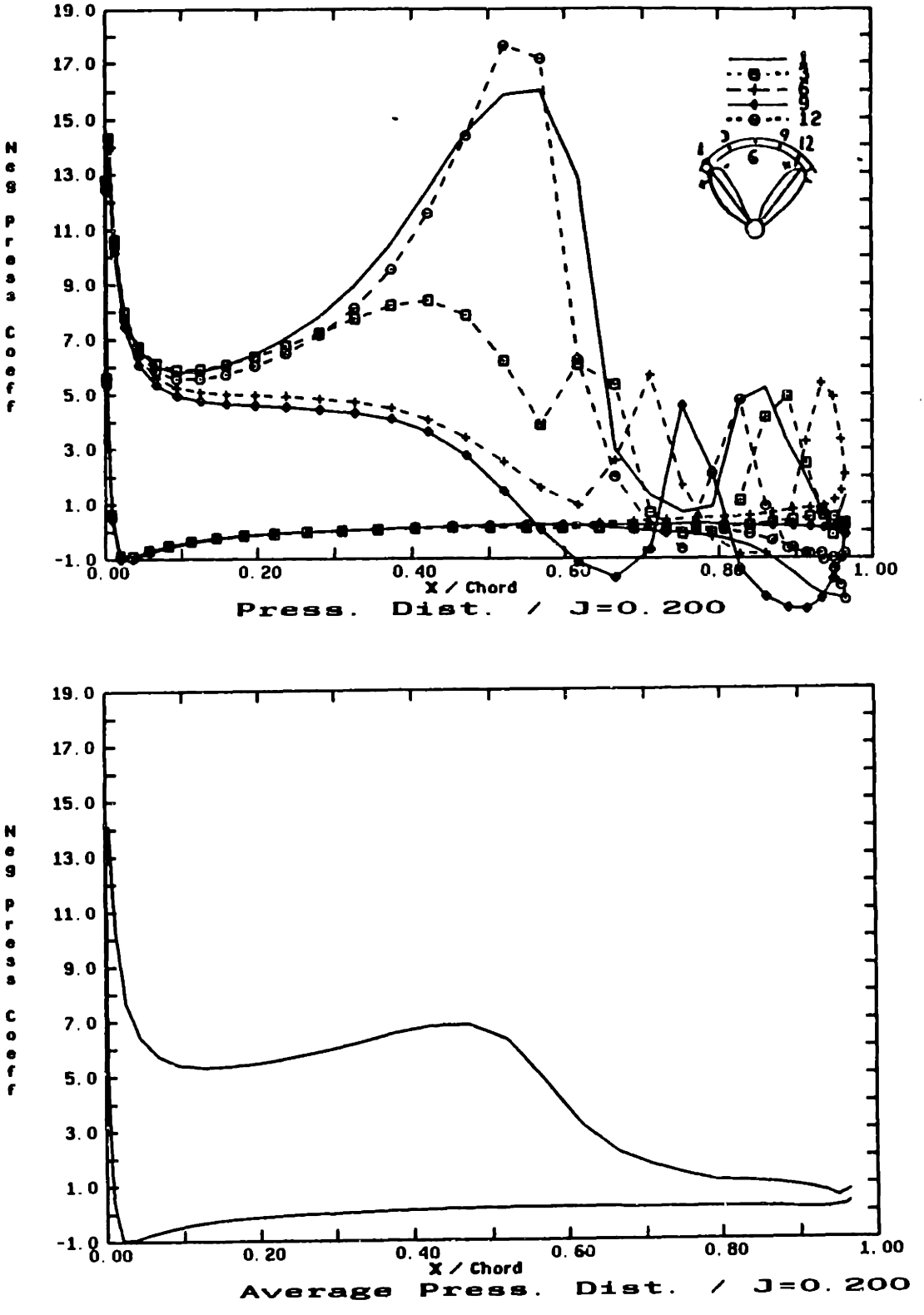

Figure D.3: Duct pressure distribution for J=0.200

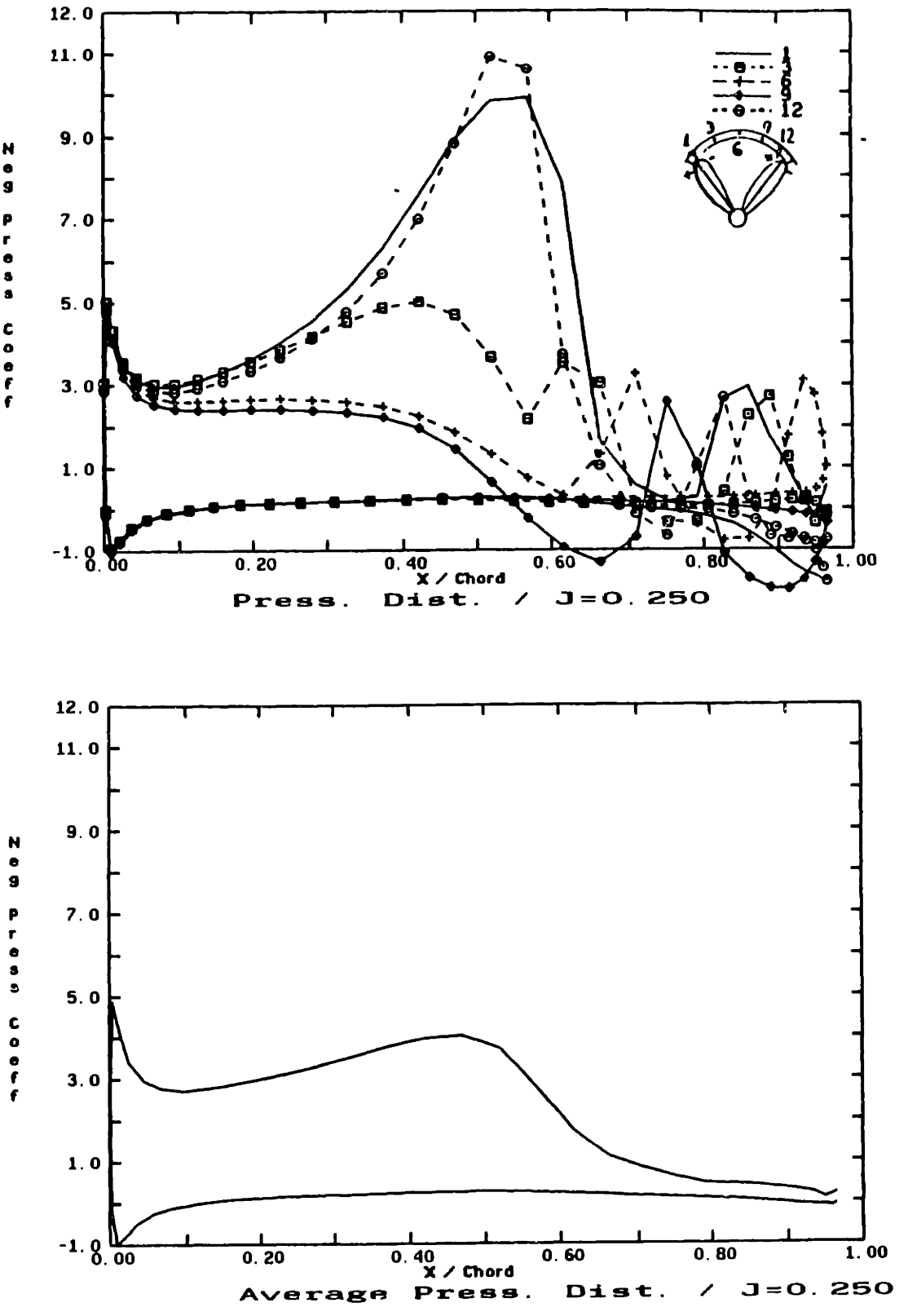

Figure D.4: Duct pressure distribution for J=0.250

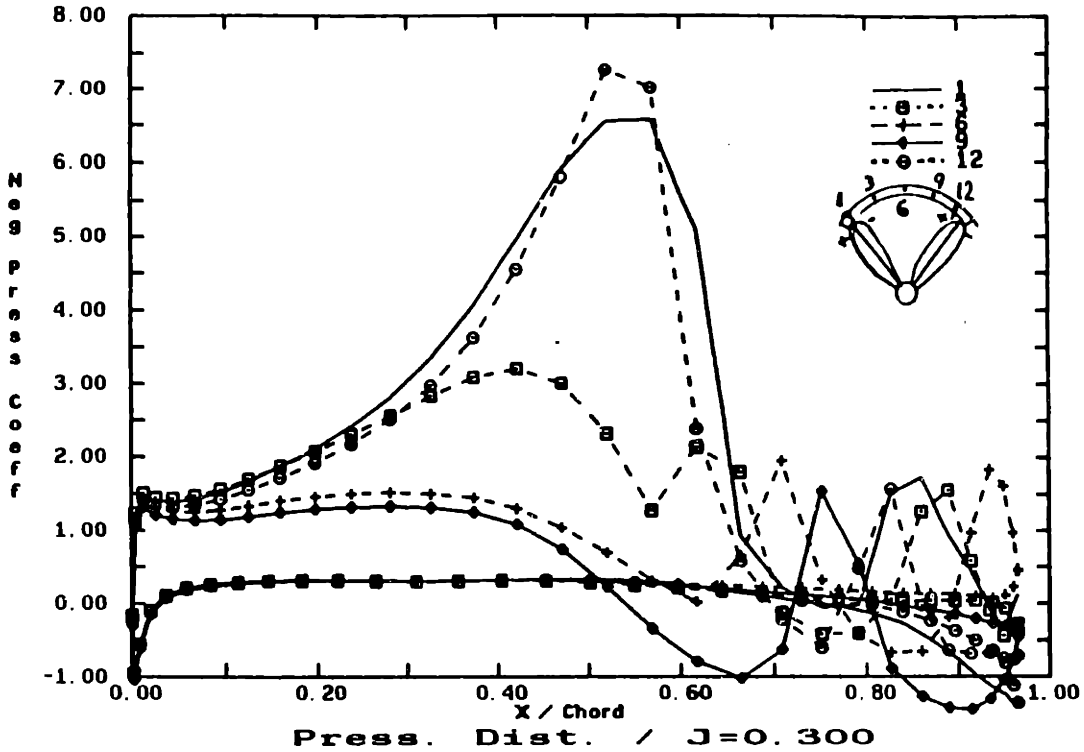

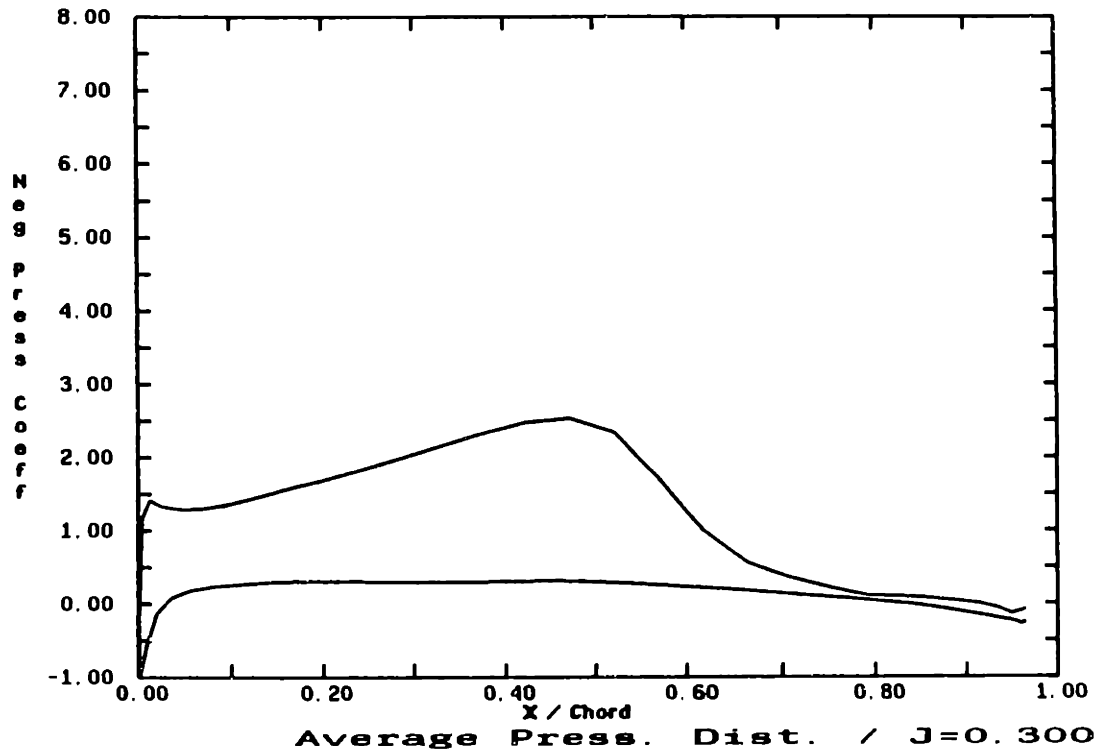

Figure D.5: Duct pressure distribution for J=0.300

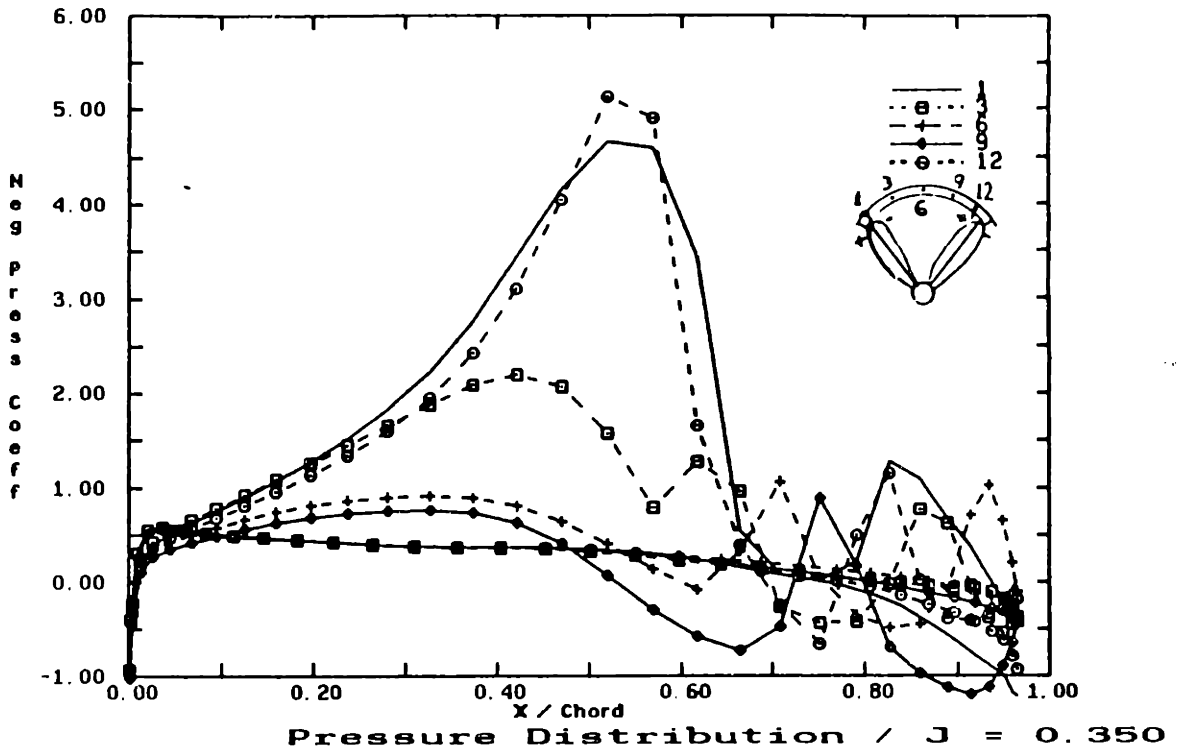

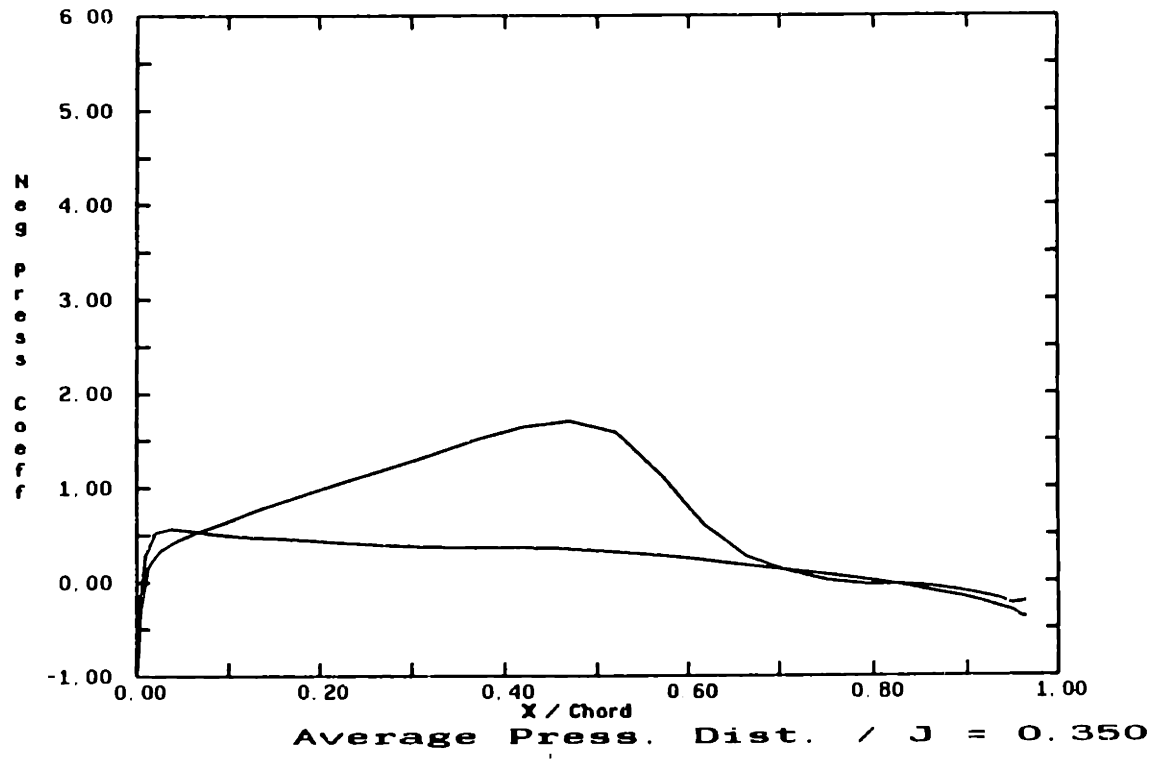

Figure D.6: Duct pressure distribution for J=0.350

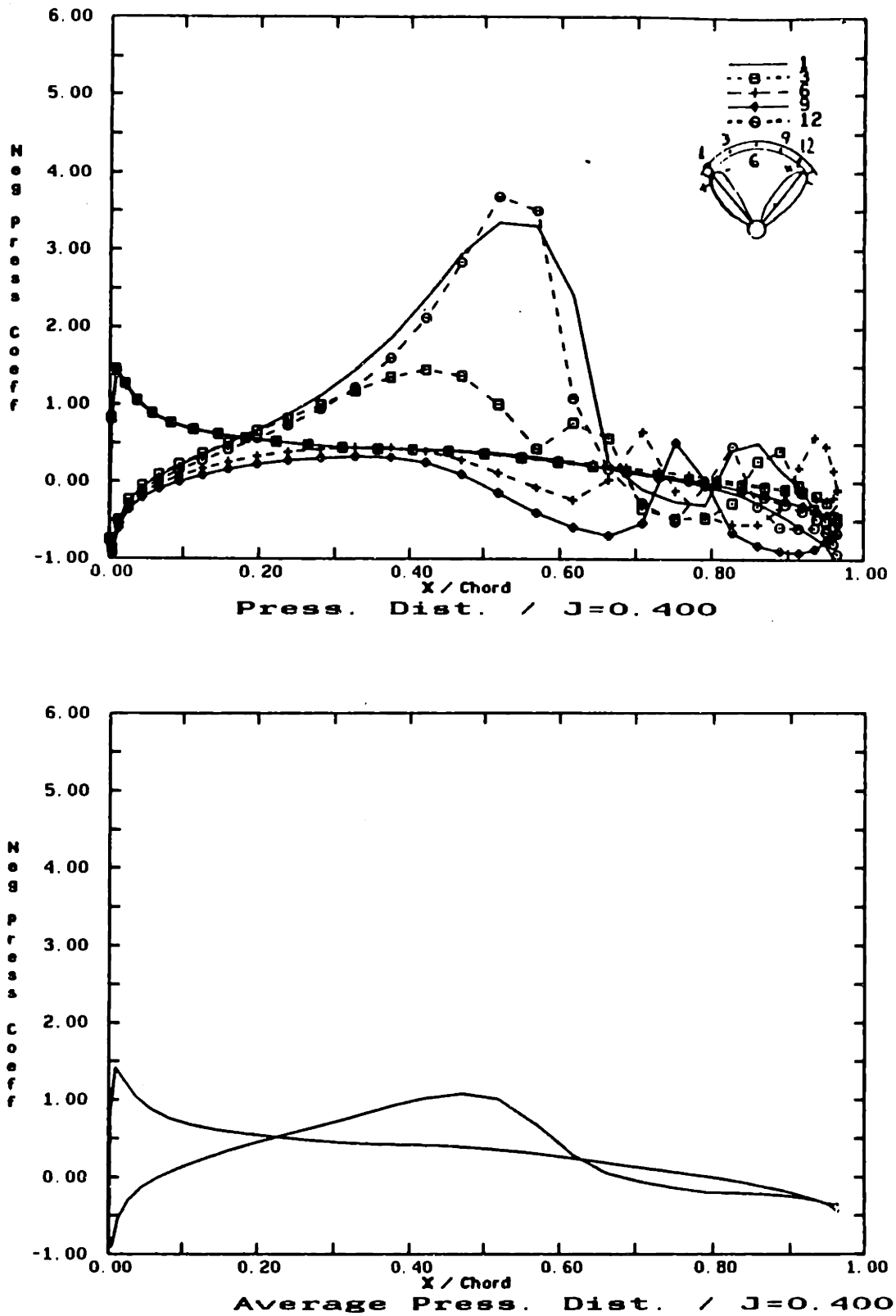

Figure D.7: Duct pressure distribution for J=0.400

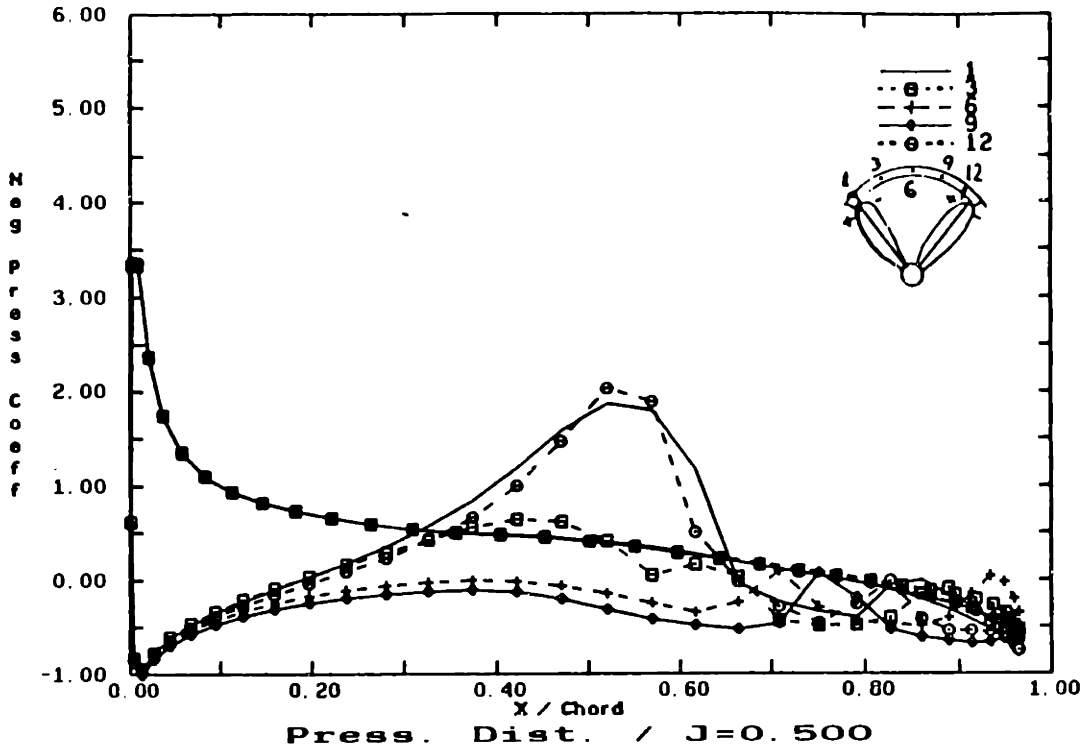

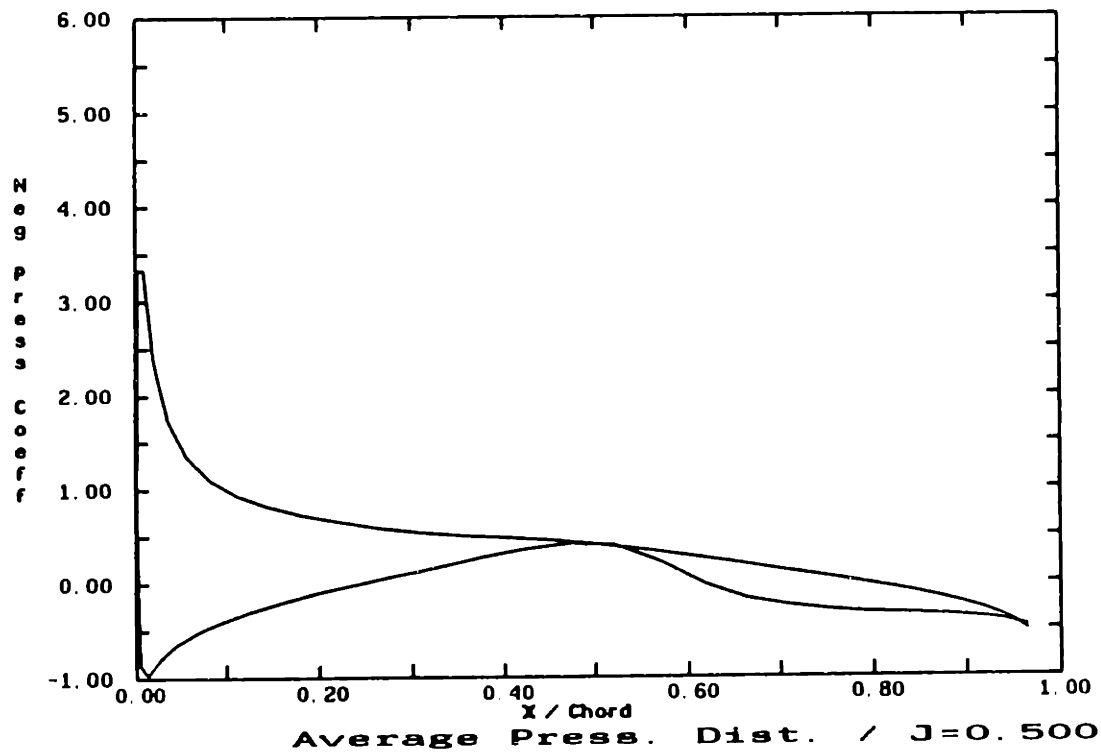

Figure D.8: Duct pressure distribution for J=0.500

Appendix E

Experimental Results

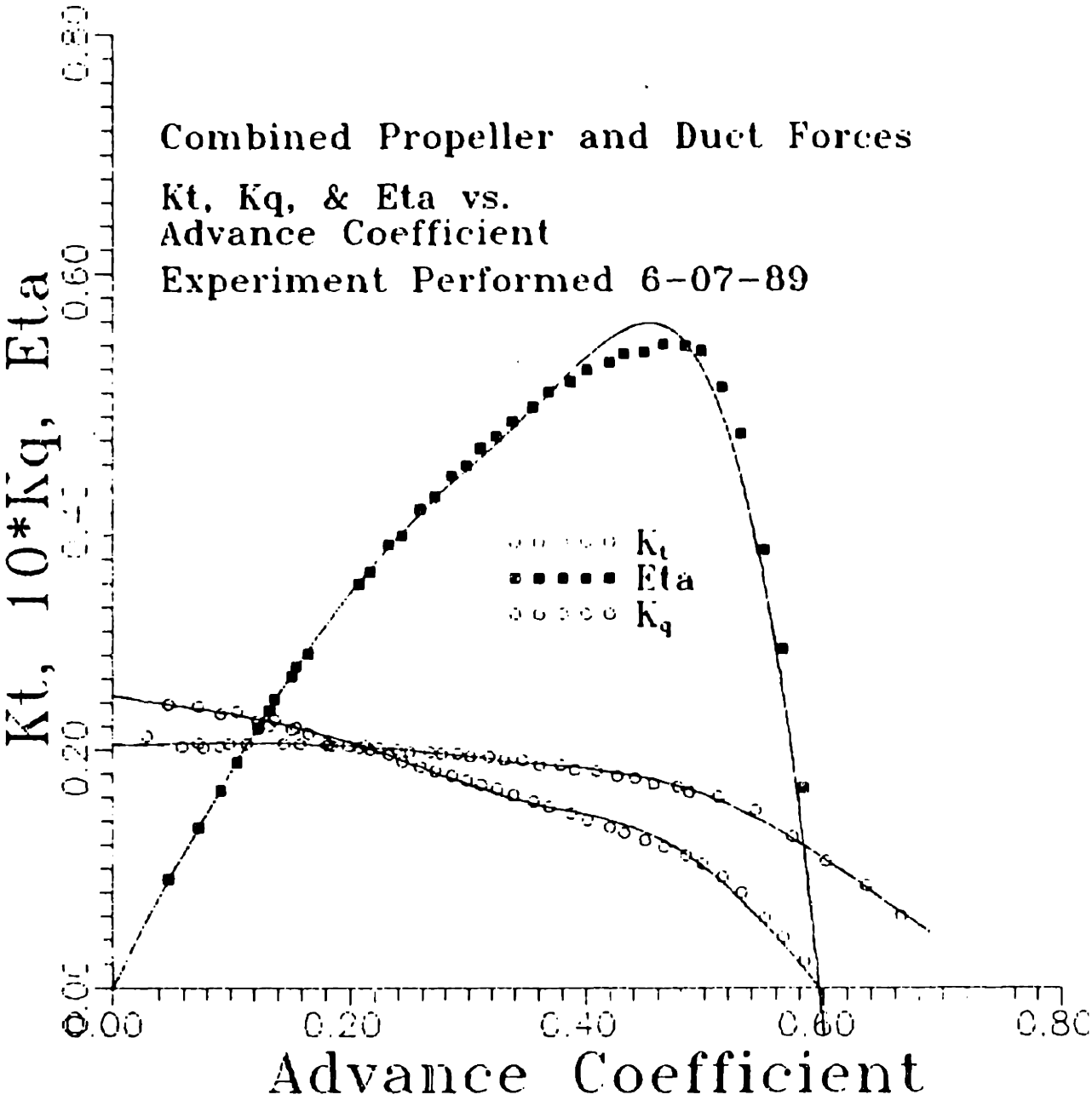

Figure E.1: Open water curve, Combined propeller and duct forces

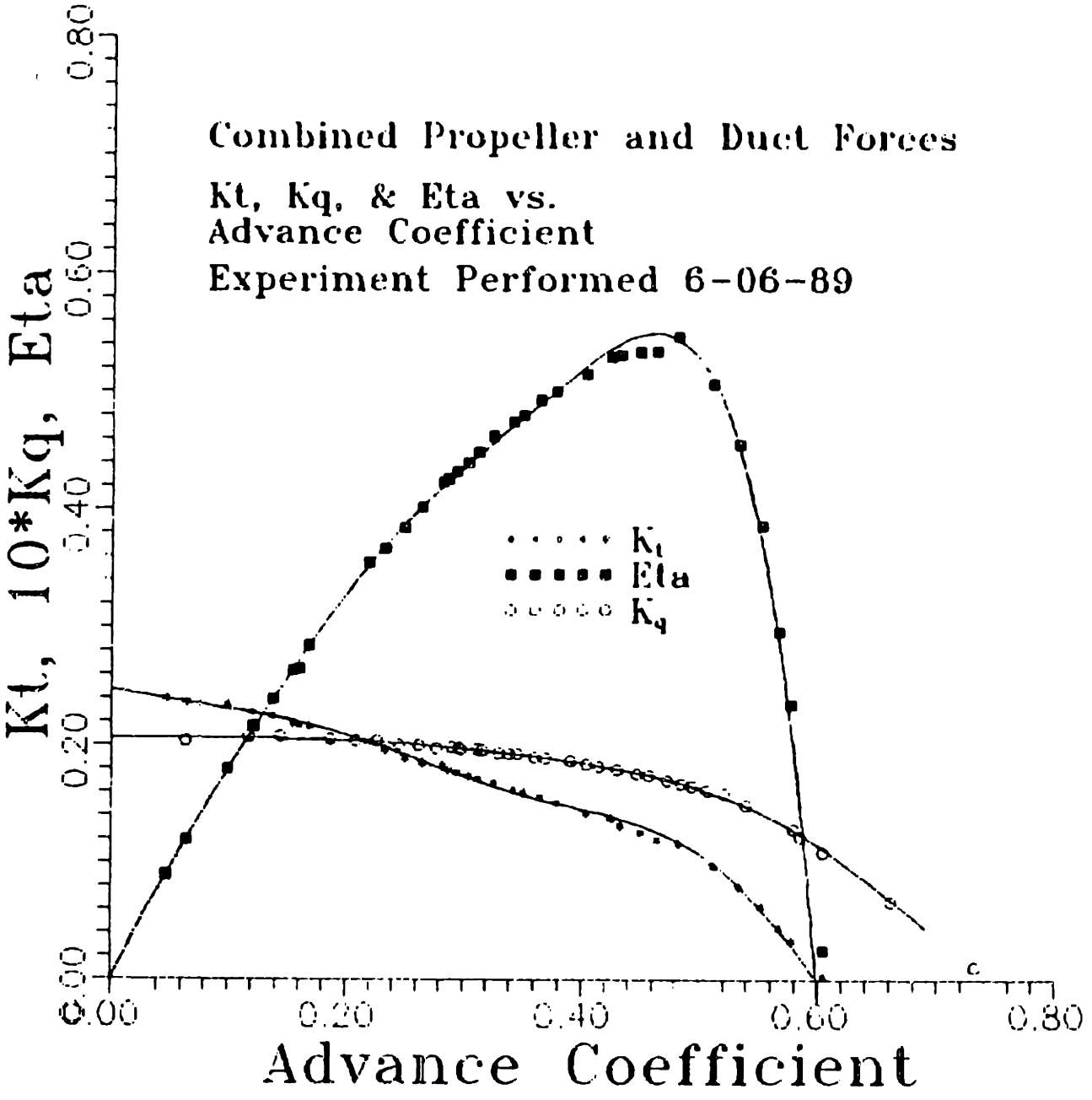

Figure E.2: Open water curve, Combined propeller and duct forces

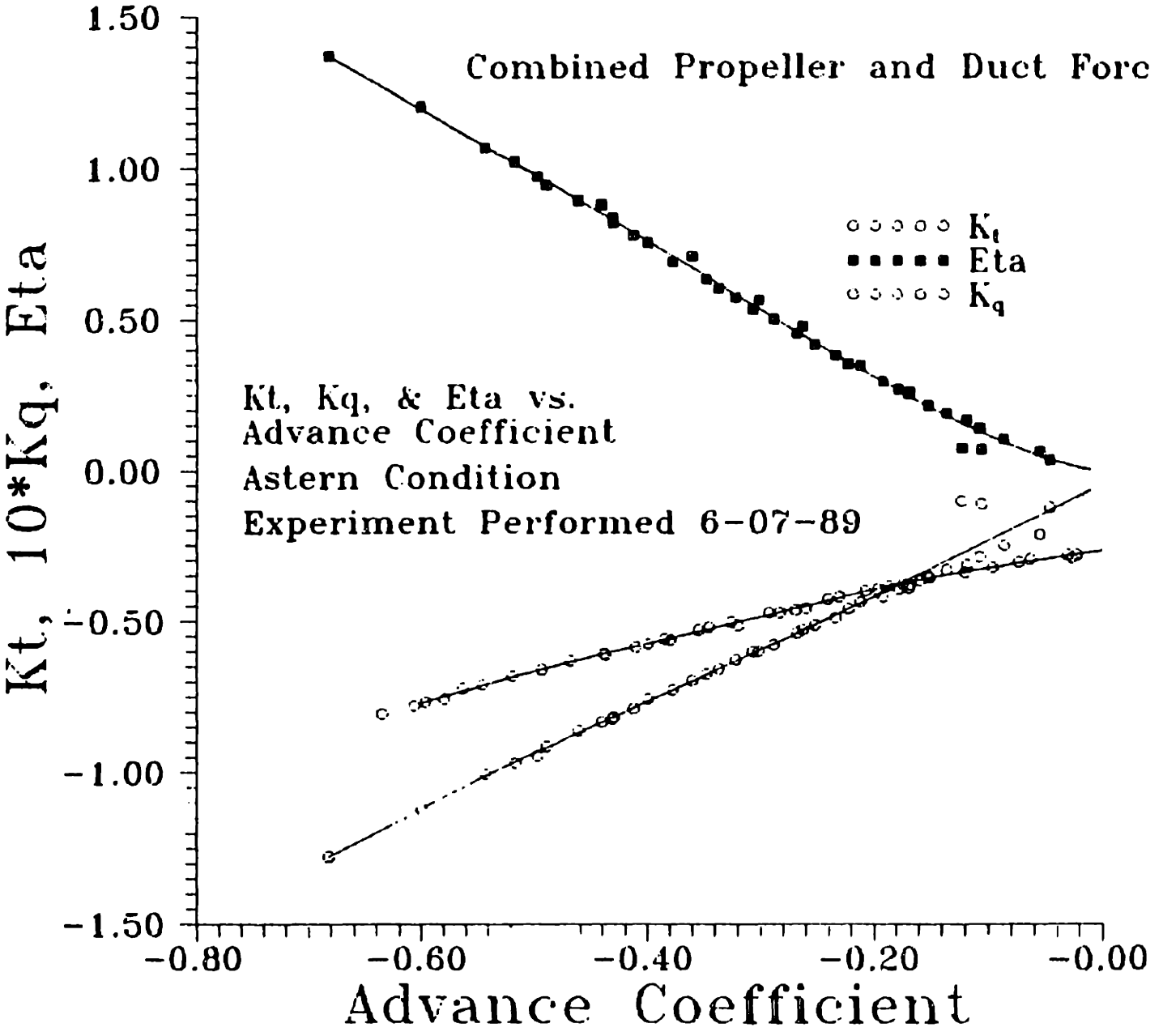

Figure E.3: Open water curve. Combined propeller and duct forces. Astern condition

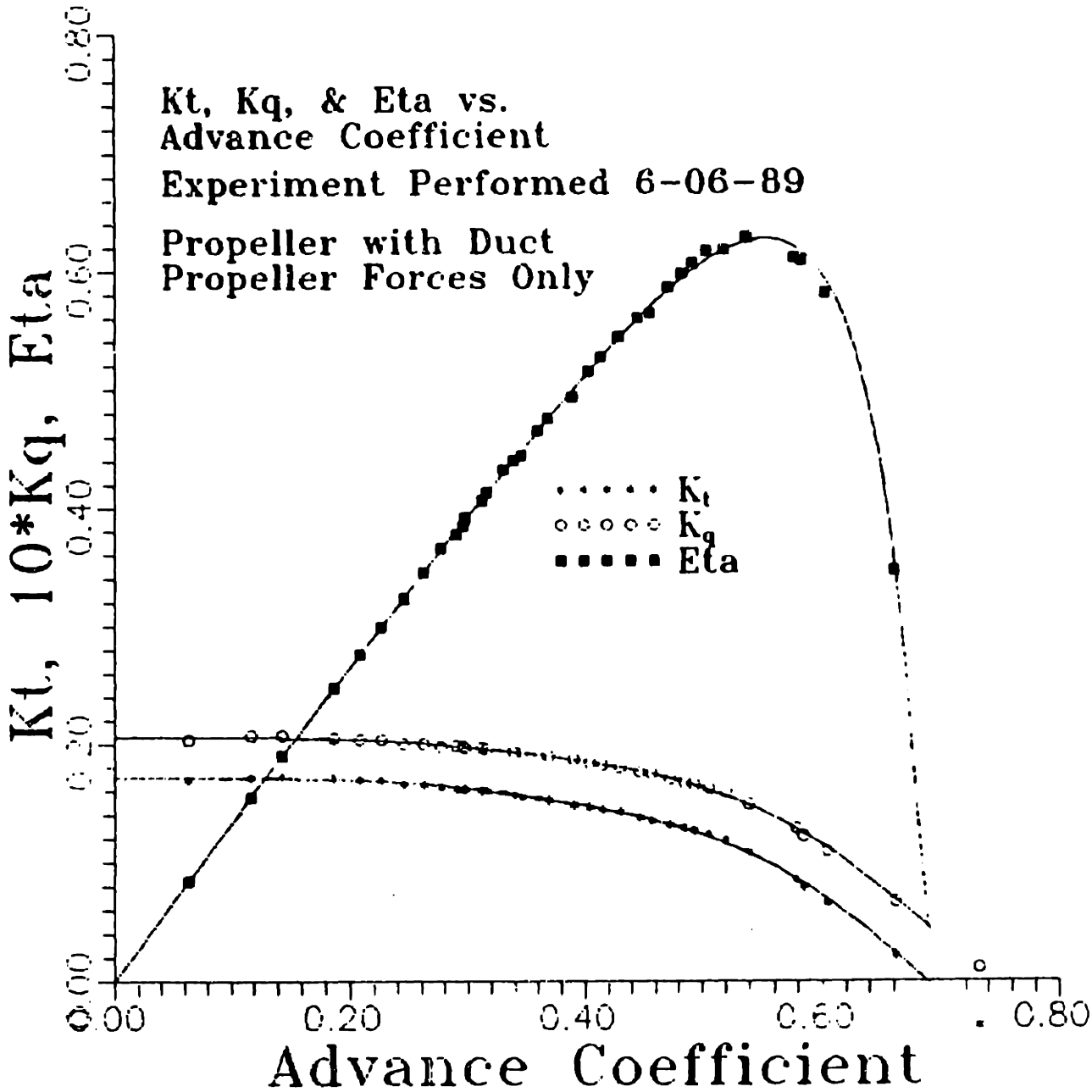

Figure E.4: Open water curve, Propeller forces only

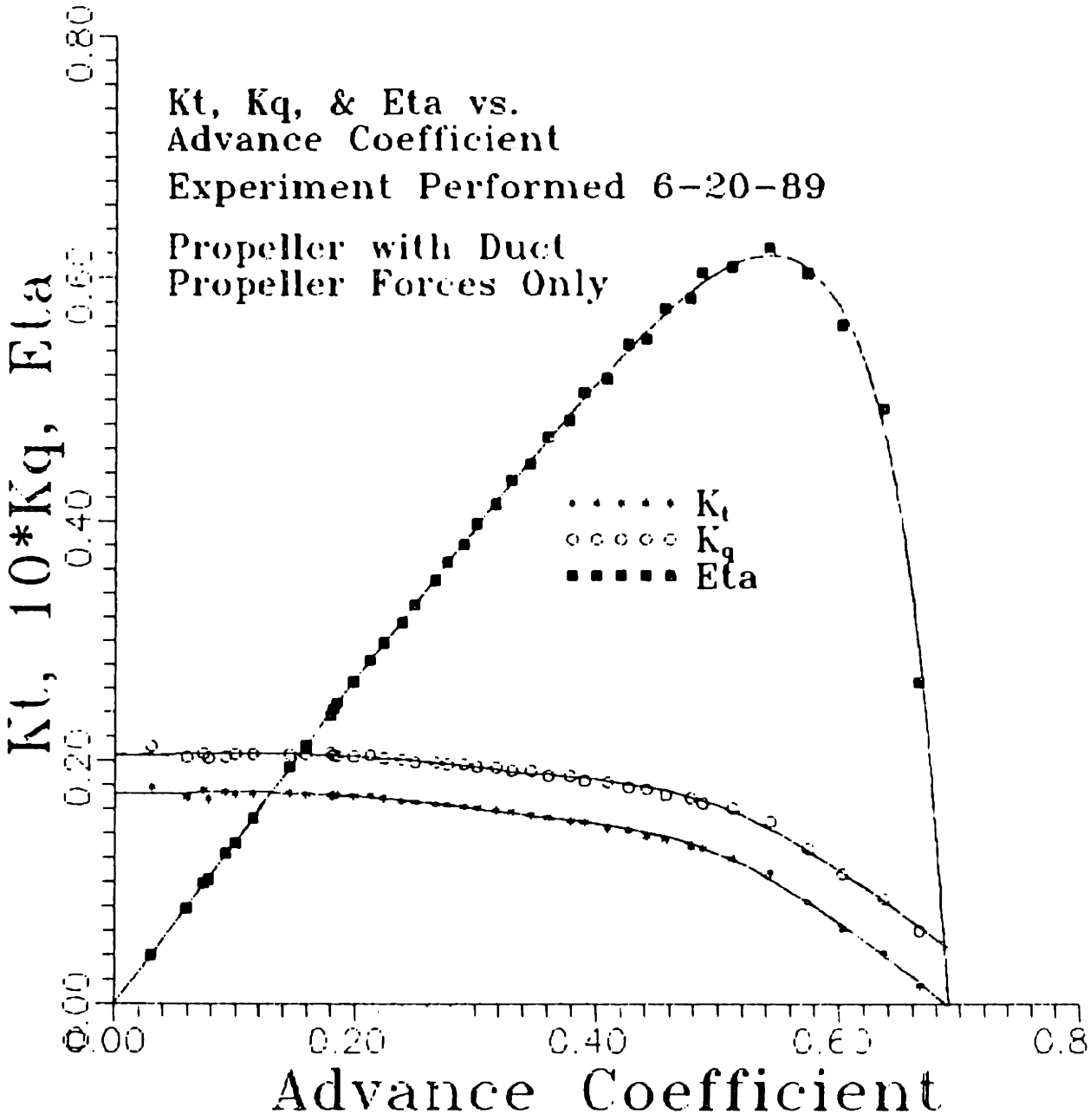

Figure E.5: Open water curve, Propeller forces only

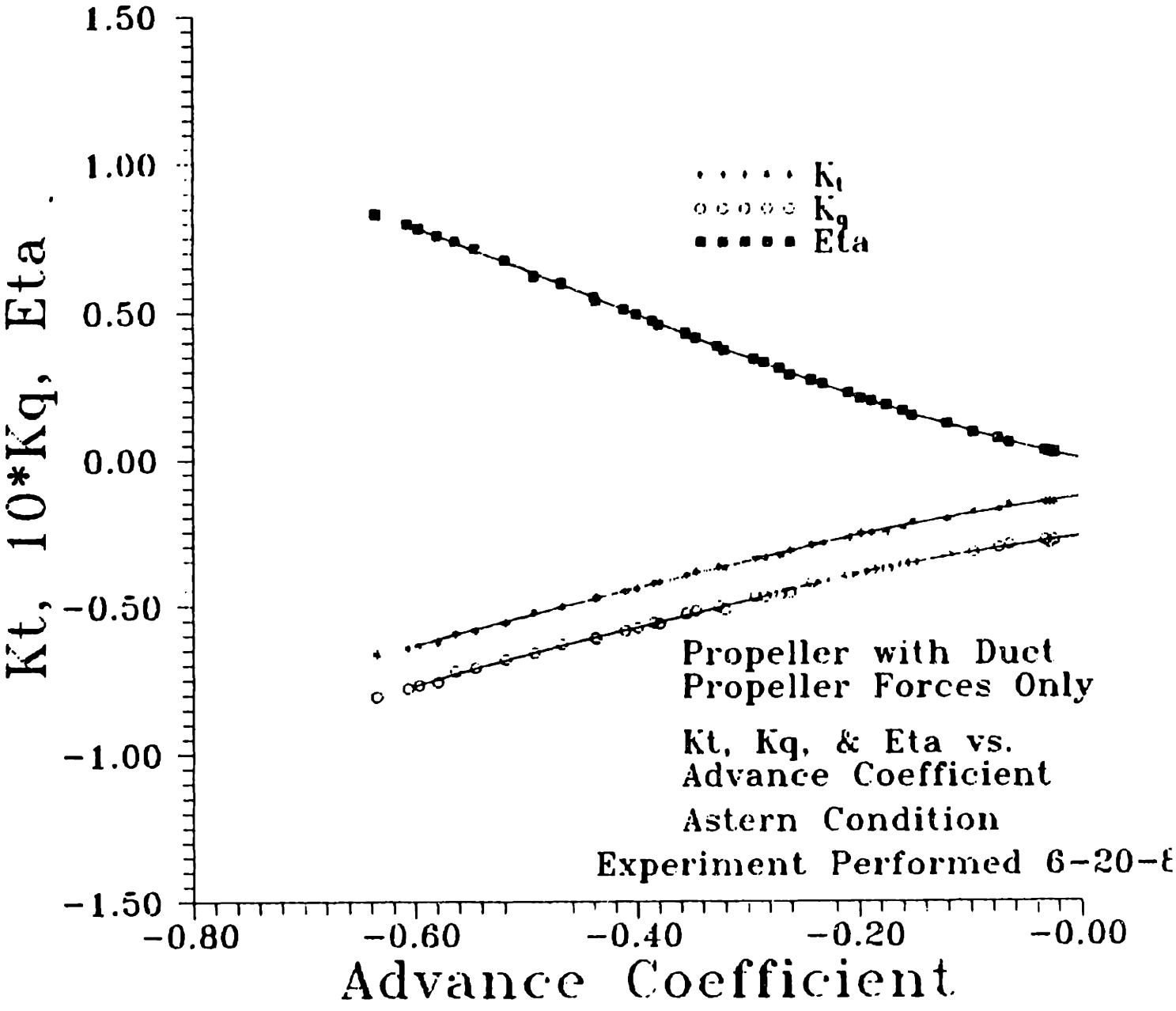

Figure E.6: Open water curve. Propeller forces only, Astern condition

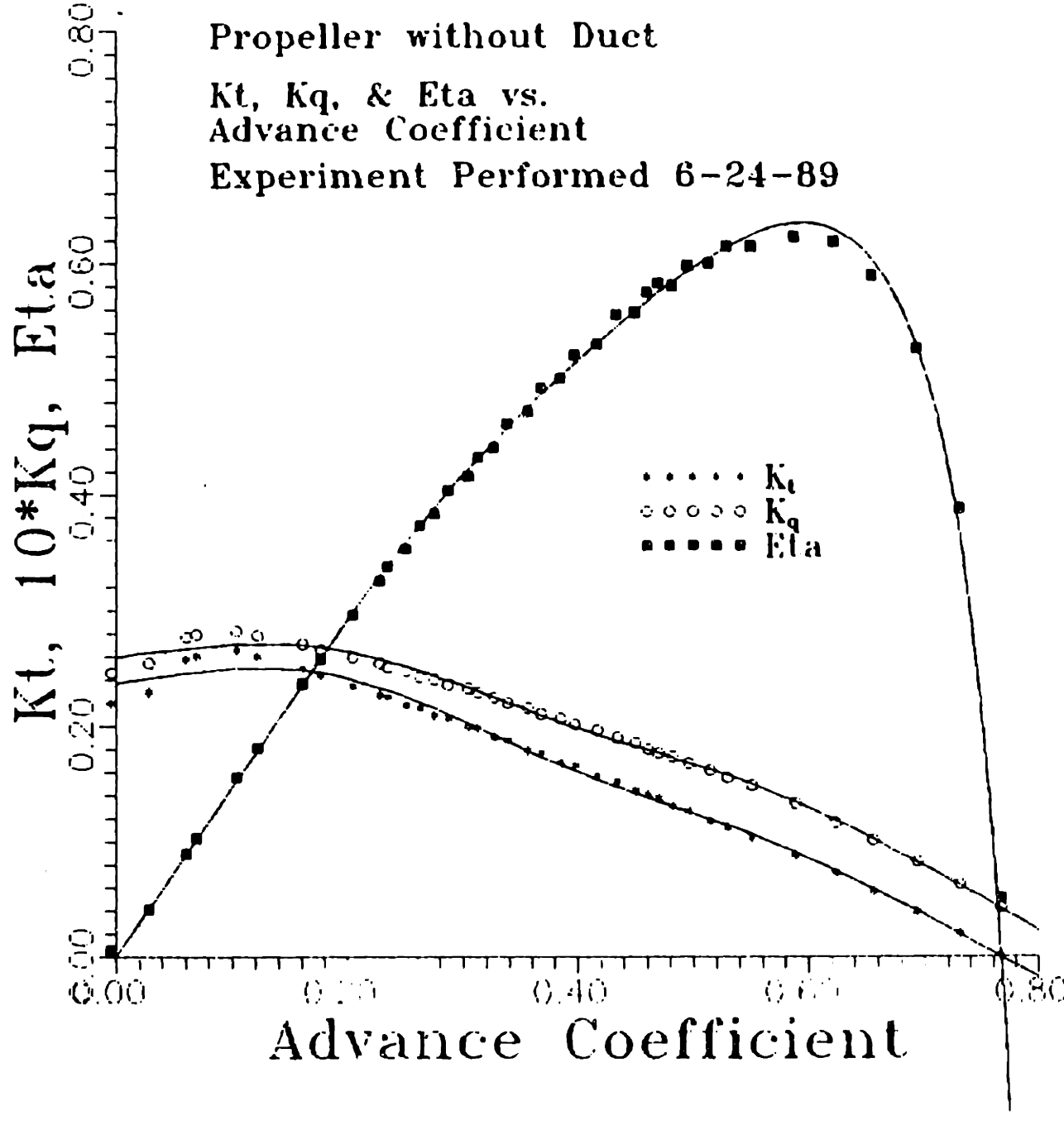

Figure E.7: Open water curve for propeller without duct

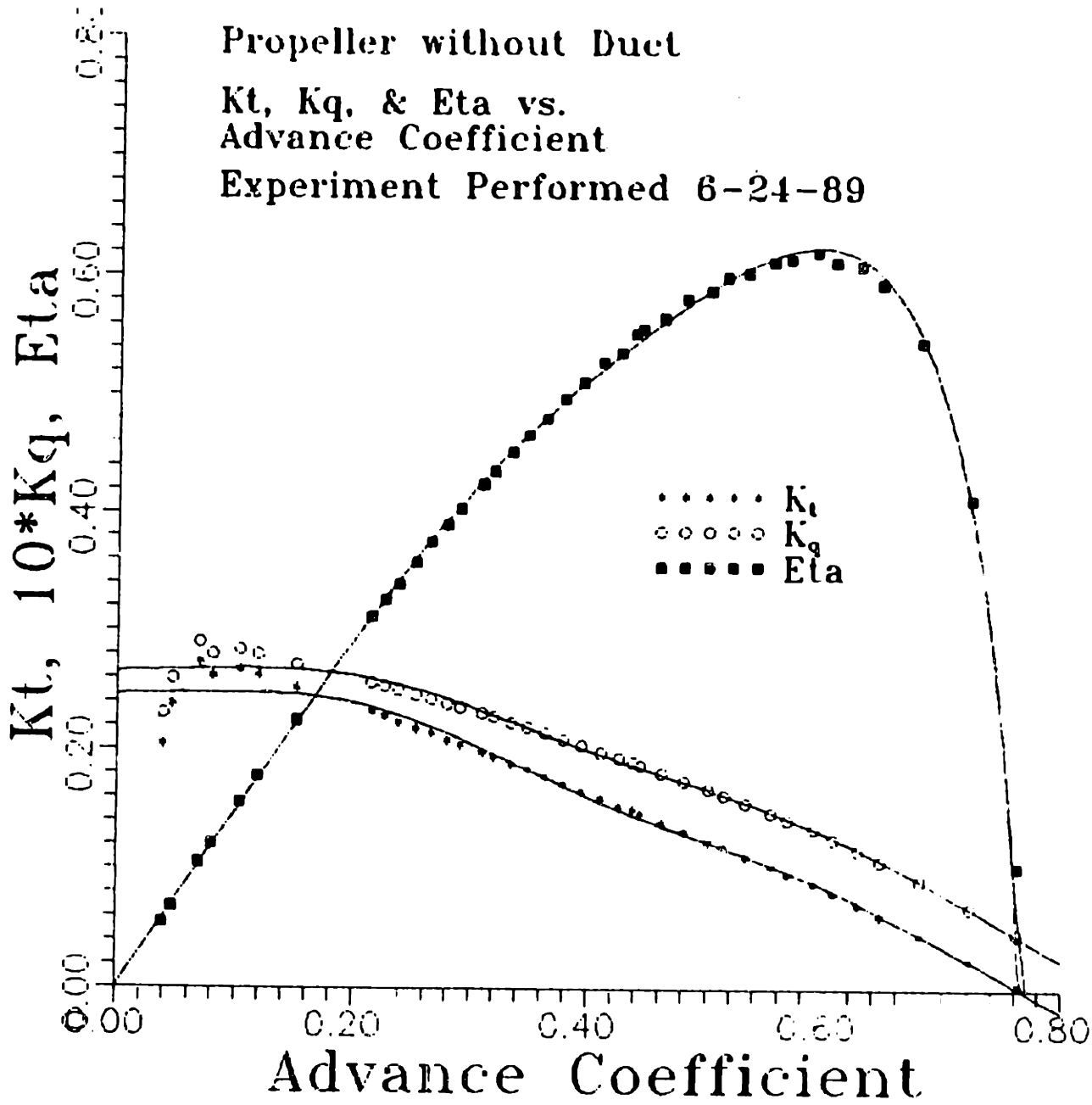

Figure E.8: Open water curve for propeller without duct

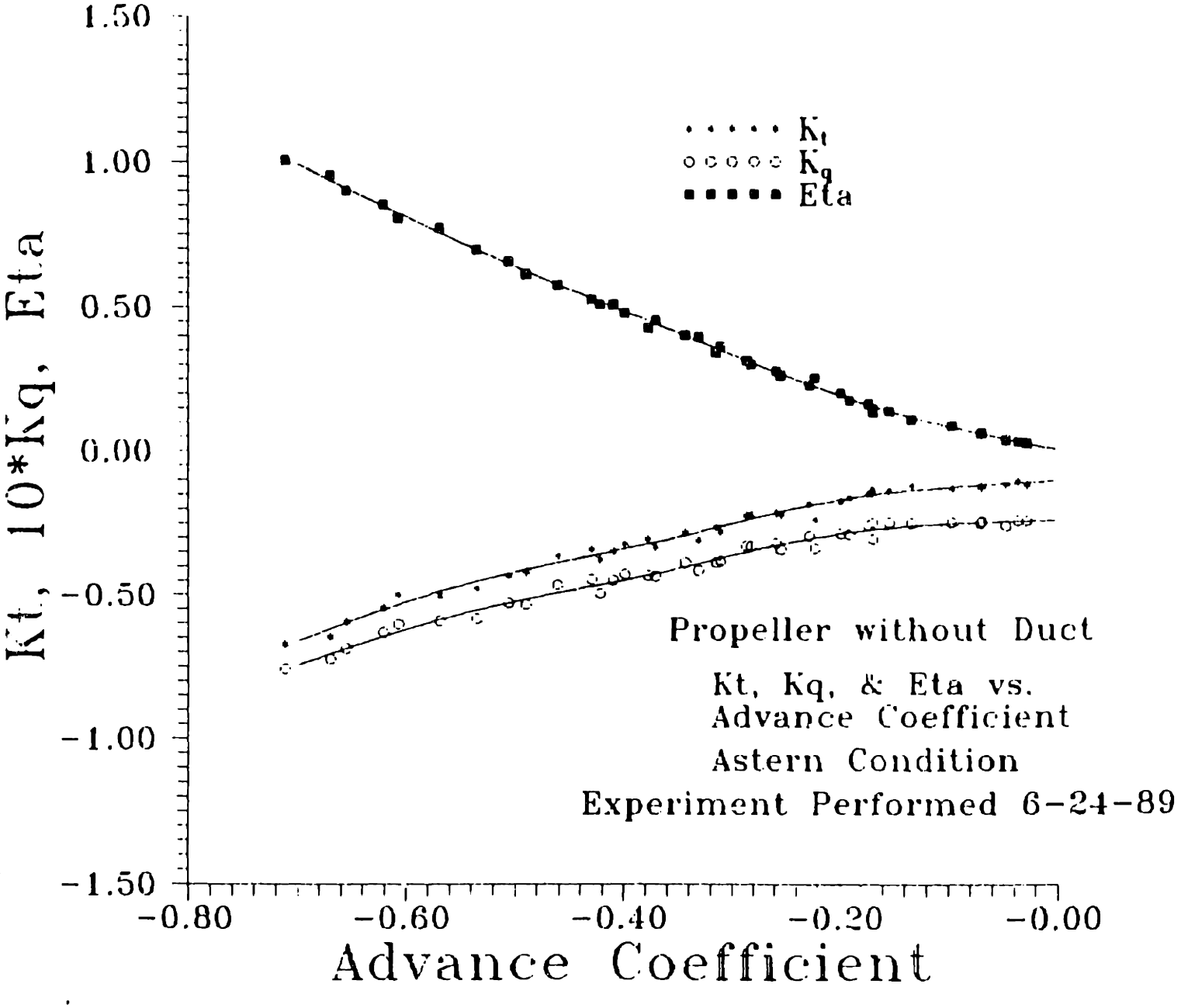

Figure E.9: Open water curve for propeller without duct, Astern condition